AN 20

CLASSIFICATION CANCELLED CONFIDENTIAL

Copy 1
RM E54I03

NACA RM E54I03

CLASSIFICATION CANCELLED

PERMANENT FILE COPY

Authority NACA RESEARCH ABSTRACTS
and Reclassification Notice No. 11
Date 8/16/52 By

RESEARCH MEMORANDUM

CLASSIFICATION CANCELLED

INVESTIGATION OF POROUS GAS-HEATED LEADING-EDGE SECTION FOR ICING PROTECTION OF A DELTA WING

By Dean T. Bowden

Lewis Flight Propulsion Laboratory
Cleveland, Ohio

CLASSIFICATION CANCELLED

CLASSIFIED DOCUMENT

This material contains information affecting the National Defense of the United States within the meaning of the espionage laws, Title 18, U.S.C., Secs. 793 and 794, the transmission or revelation of which in any manner to an unauthorized person is prohibited by law.

NATIONAL ADVISORY COMMITTEE
FOR AERONAUTICS

WASHINGTON

January 19, 1955

FILE COPY
To be returned to
the files of the National
Advisory Committee
for Aeronautics
Washington, D. C.

CLASSIFICATION CANCELLED CONFIDENTIAL

CLASSIFICATION CANCELLED

NATIONAL ADVISORY COMMITTEE FOR AERONAUTICS

RESEARCH MEMORANDUM

INVESTIGATION OF POROUS GAS-HEATED LEADING-EDGE SECTION FOR ICING PROTECTION OF A DELTA WING

By Dean T. Bowden

SUMMARY

A tip section of a delta wing having an NACA 0004-65 airfoil section and a 60° leading-edge sweepback was equipped with a porous leading-edge section through which hot gas was bled for anti-icing. Heating rates for anti-icing were determined for a wide range of icing conditions. The effects of gas flow through the porous leading-edge section on airfoil pressure distribution and drag in dry air were investigated. The drag increase caused by an ice formation on the unheated airfoil was measured for several icing conditions. Experimental porous surface- to free-stream convective heat-transfer coefficients were obtained in dry air and compared with theory.

Adequate icing protection was obtained at all icing conditions investigated. Savings in total gas-flow rate up to 42 percent may be obtained with no loss in anti-icing effectiveness by sealing half the upper-surface porous area. Gas flow through the leading-edge section had no appreciable effect on airfoil pressure distribution. The airfoil section drag increased slightly (5-percent average) with gas flow through the porous surface. A heavy glaze-ice formation produced after 10 minutes of icing caused an increase in section drag coefficient of 240 percent. Experimental convective heat-transfer coefficients obtained with hot-gas flow through the porous area in dry air and turbulent flow were 20 to 30 percent lower than the theoretical values for a solid surface under similar conditions. The transition region from laminar to turbulent flow moved forward as the ratio of gas velocity through the porous surface to air-stream velocity was increased.

INTRODUCTION

An airfoil may be protected in icing conditions by heating the leading-edge section so that all impinging water is evaporated. The required heat is usually obtained either by use of electric heating blankets or hot gas flowing through chordwise passages in contact with

CLASSIFICATION CANCELLED

the inner surface of the wing skin. Increasing speeds of present-day aircraft have resulted in very large heating rates for this method of protection (ref. 1), requiring either large generating capacity for an electric system or high gas-flow rates for a gas-heated system. One means of reducing these heating requirements is by the use of a cyclic de-icing system. Research on such systems (refs. 2 and 3) has shown a reduction in heat requirement over continuous heating systems. For a high-speed thin-wing aircraft, considerations of available space, weight, complexity, and limited time in icing may require the use of a continuous heating system in spite of the higher heating requirements. The required surface heat release may be achieved in an economical manner by using a porous-metal leading-edge section through which hot gas is bled. Since the porous metal provides a large hot-gas contact area, the temperature of the porous surface is the same as that of the gas leaving the wing. With a conventional system having chordwise channels, the temperature of the gas leaving the channels is higher than the outer-skin temperature, and heat is wasted. Where space is limited, the porous surface has the additional advantage of attaining a high heat-release rate in a relatively short heated length.

The use of a porous-skin heating system, however, may have effects on airfoil lift and drag. These effects may be measured experimentally to determine whether or not they are important. Contamination of the porous area by dust and insects may also be a problem. Periodic cleaning of the porous surfaces may be an acceptable solution.

Some experimental data on the use of a porous wall for heating are available. An experimental and theoretical investigation using a porous flat plate is reported in reference 4. A comparison between a porous-skin heating system for icing protection and a double-skin system with chordwise channels was made in reference 5 for one icing condition and indicates that the porous system is the more efficient of the two.

The associated field of transpiration cooling, wherein air is used to cool a porous wall in contact with a hot gas, has received much greater attention, both experimentally and theoretically (refs. 6 to 10). The superiority of transpiration cooling over convection cooling is shown in reference 8. Heat-transfer coefficients for laminar and turbulent flow may be obtained from the transpiration-cooling literature and applied to the problem of porous-wall heating provided the surface to free-stream temperature difference is small. The transition region from laminar to turbulent flow usually must be located experimentally for a particular body.

The present investigation was conducted in the NACA Lewis icing research tunnel using an airfoil model provided by an aircraft manufacturer. The influence of the porous system on airfoil pressure distribution, drag, and heat transfer was determined in dry air. Drag of the airfoil in icing with no heat was investigated to establish the need for icing protection. Heating requirements of the porous system for anti-icing were determined, and system performance was observed for a wide range of icing conditions. The de-icing characteristics of the porous leading-edge system were investigated briefly.

DESCRIPTION OF MODEL AND EQUIPMENT

The airfoil model used in this study was a tip section of a delta plan-form wing, having an NACA 0004-65 airfoil section in a plane parallel to the air stream with a root chord of 155.5 inches, a 60° leading-edge sweepback, and a span of 87 inches. (All spanwise dimensions used herein are measured normal to the air-stream direction unless otherwise noted.) The model was mounted horizontally on the sidewall of the 6- by 9-foot icing research tunnel (fig. 1) and was supported near the tip by telescoping support struts. The porous leading-edge section was formed from 0.040-inch-thick porous sintered stainless steel sheets, riveted to stainless steel ribs and baffle. A schematic view of the wing and leading-edge section is shown in figure 2. All joints were made pressure-tight by sealing with a silicon rubber compound which was cured in place at high temperature. The chordwise extent of heated area on both upper and lower surfaces was varied from 8 inches at the root to 6.5 inches near the tip (fig. 2). The leading-edge hot-gas delivery tube extended to midspan of the wing model; 1/4-inch diameter holes spaced about 8 inches apart were drilled in the rear of the tube (facing the baffle) to allow hot gas to flow into the D-duct. The end of the tube was open to allow gas to flow to the leading-edge section outboard of the midspan. After preliminary tests an additional section of tubing was added, which was approximately 3 feet long with 1/8-inch holes spaced 2 inches apart drilled in the forward part of the tube (facing the leading edge). No insulation was provided in the leading-edge section other than the air gap formed by the space between the baffle and the spar (fig. 2). The nonporous portion of the airfoil skin was provided with internal electric heaters for prevention of frost during the study of drag associated with ice accumulations.

Model instrumentation consisted of static-pressure taps and thermocouples at various spanwise stations (table I and fig. 2) on the airfoil surface, in the hot-gas delivery tube, and in the leading-edge D-duct. Thermocouples were also available to measure structural temperatures (baffle, spar, and ribs). The porous surface thermocouples were installed by inserting the iron and constantan wires into holes drilled through the porous metal about 1/4-inch apart, then spotting each wire in place with silver solder.

Airfoil drag was determined at three spanwise stations (table I) by means of a movable wake-survey rake. The wake rake was located at 25-percent chord behind the airfoil for each spanwise station, and consisted of 80 electrically heated total-pressure tubes and five static-pressure tubes. The total-pressure tubes were spaced on 1/4-inch centers; the static-pressure tubes were spaced on 5-inch centers.

Measurements of tunnel airspeed, angle of attack, and total air temperature were obtained from standard tunnel instrumentation. Liquid-water content was determined by means of a pressure-type icing-rate meter. Icing cloud droplet size and distribution were determined from a previous calibration obtained by employing water droplets carrying dye in solution.

Flow calibration of the porous leading edges for various spanwise and chordwise stations was obtained from reference 11.

CONDITIONS AND PROCEDURE

The range of conditions covered in this investigation was as follows:

Airspeed, mph	150 to 275
Angle of attack, deg	0 to 8
Air total temperature, ^{o}F	0 to 25
Liquid-water content, g/cu m	0.3 to 1.0
Mean effective droplet diameter, microns (micron = 3.28×10^{-6} ft)	9 to 15
Pressure altitude, ft	1500 to 3500
Inlet gas temperature at leading edge, ^{o}F	330 to 530
Gas-flow rate, lb/(hr)(ft span)	40 to 170

Datum air temperature, which is the average surface temperature of the unheated airfoil leading-edge section in wet air, was found to be essentially equal to the air total temperature for the range of conditions investigated.

Airfoil pressure distribution and drag in dry air were determined for two nominal airspeeds and for angles of attack of 0^{o} to 8^{o} at three spanwise stations under the following conditions: (a) no gas flow through porous area, (b) a gas-flow rate of 135 pounds per hour per foot span, and (c) no gas flow and porous area sealed with a plastic material.

Experimental surface- to free-stream convective heat-transfer coefficients were determined for airspeeds of 175 and 275 miles per hour, angles of attack of 0^{o} and 2^{o}, and several heating rates at station C (48.3-in. chord) in dry air by measurement of local temperatures and gas-flow rates.

The local gas-flow rates through the porous metal were determined by means of the flow calibration data obtained from reference 11, which were replotted in terms of $(p_1^2 - p_2^2)/\mu^2 T\tau$ against $\gamma v/\mu$, as suggested in reference 12. (All symbols are defined in the appendix.) By means of this correlation, the flow calibration data obtained at constant temperature and constant external pressure p_2 may be used for a wide range of temperature and external pressure. Typical flow correlation curves are presented in figure 3 for station A. For a particular location and total gas-flow rate, the local gas-flow rate was calculated by evaluating the term $(p_1^2 - p_2^2)/\mu^2 T\tau$, obtaining the term $\gamma v/\mu$ from the appropriate flow correlation curve, and multiplying $\gamma v/\mu$ by μ to obtain γv, the local gas-flow rate in pounds per second per square foot. The internal pressure p_1 was obtained from static-pressure taps inside the D-duct, while the external surface pressure p_2 was calculated from the experimentally determined airfoil pressure distribution. Ideally, the gas temperature and viscosity used with the correlation curves should be obtained at the midwall of the porous-metal skin. The midwall gas temperature, however, was not available from the instrumentation; consequently, the external surface temperature was used, since it ordinarily does not differ greatly from the midwall gas temperature. The accuracy of the local gas-flow rates was determined by integrating the local flow rates chordwise and spanwise to obtain a total gas-flow rate, and comparing this total flow rate to the flow rate measured by an orifice in the hot-gas supply line.

Airfoil drag was determined at an airspeed of 275 miles per hour for several icing conditions at angles of attack of 2° to 6° with the leading-edge section unheated, and for one icing condition at an angle of attack of 2° with runback icing on the lower surface resulting from submarginal heating. The airfoil afterbody (nonporous area of the wing) was heated at all times during the icing drag determinations to prevent the formation of frost due to tunnel air-stream turbulence and supersaturation. Because of difficulties in moving the wake rake during icing, most of the icing drag information was obtained at station B (83.8-in. chord). When possible, values were obtained at stations A and C near the end of the icing period.

In the study of anti-icing heat requirements, the usual procedure was to set a particular icing condition and a heating rate higher than necessary for complete ice prevention. The inlet-gas temperature was then maintained constant, and the gas-flow rate was diminished in several steps until the heating system no longer gave adequate protection. At each setting of gas flow, system performance was observed for approximately 15 minutes, and a complete record was made of all pertinent data, including photographs of residual ice formations.

RESULTS AND DISCUSSION

Characteristics of Porous System in Dry Air

In order to determine any adverse aerodynamic effects due to use of the porous system, airfoil pressure distribution and drag were measured in dry air with and without gas flow through the porous area and with the porous area sealed. The effect of hot gas flow on surface- to free-stream convective heat-transfer coefficients was investigated by comparing the experimental coefficients obtained in dry air with hot gas flow with available theory for solid and porous flat plates. These results are presented in the following sections.

Effect of porous system on airfoil pressure distribution and drag. - Experimental pressure distributions were obtained at two airspeed ranges (150 to 175 and 200 to 250 mph) with no gas flow, and with a gas-flow rate corresponding to the maximum used for anti-icing (135 lb/(hr)(ft span)). Gas flow had no effect on pressure distribution at angles of attack of 0°, 2°, and 4°. Minor changes in airfoil pressure distribution on the upper surface were noted at station C for an angle of attack of 6°, and at stations B and C for an angle of attack of 8°. These results are shown in figure 4 for the airspeed range of 150 to 175 miles per hour. The areas enclosed by the pressure diagrams for gas flow and no gas flow are equal within 1 to 2 percent; consequently, no appreciable change in lift will result from gas flow through the porous area.

The pressure distribution was also measured with the porous area sealed by a plastic material for angles of attack of 2° and 6°. The pressure distribution with the porous area sealed was found to be the same as with the porous area open and no gas flow.

It may be concluded that, for the conditions of this investigation, the use of the porous leading-edge anti-icing system has no detrimental effects on airfoil pressure distribution.

The effect of maximum gas-flow rate (135 lb/(hr)(ft span)) on airfoil drag is shown in figure 5. Generally, the airfoil drag is slightly higher with gas flow than with no gas flow, although a decrease in airfoil drag with gas flow is noted at an angle of attack of 6° for stations A and C. The average increase in airfoil drag with gas flow for the data of figure 5 is approximately 5 percent. This increase may be associated with the forward movement of the transition region from laminar to turbulent flow, which is shown in reference 13 to be a function of gas- to air-stream-velocity ratio.

The effect on airfoil drag coefficient of sealing the porous area was measured at angles of attack of 2° and 6°. Within the accuracy of the data, the airfoil drag coefficients obtained with the porous area sealed were the same as with the porous area not sealed and no gas flow.

Dry-air heat transfer. - Calculations by the method of references 4 and 9 show that, for the range of air stream and gas velocities in this report, the surface- to free-stream convective heat-transfer coefficient for turbulent flow may be 10 to 25 percent less for a porous skin with gas flow than for a solid skin. As a result of the decreased surface- to free-stream heat-transfer coefficient, the porous-skin heating system will require a lower gas-flow rate to maintain a given airfoil surface temperature than a heating system utilizing a solid skin. Gas-flow requirements are further minimized by the porous system because of the large hot-gas contact area provided by the many minute gas passages in the metal. The temperature of the gas leaving the porous surface is equal to that of the porous surface, while in a conventional system having chordwise channels the temperature of the gas leaving the channels usually is higher than the outer surface temperature, and heat is wasted.

In the present investigation, experimental surface- to free-stream convective heat-transfer coefficients were obtained in dry air and compared with theoretical values calculated from references 4 and 9 for a porous flat plate in turbulent flow and from reference 14 for a solid flat plate in laminar and turbulent flow. A heat balance was made at the outer surface of the porous skin, neglecting conduction into the wing structure and using local values of temperature and gas-flow rate as follows:

$$3600\ \gamma_g v_g c_p t_{g,D} = 3600\ \gamma_g v_g c_p t_s + h(t_s - t_d) \qquad (1)$$

Solving for the convective heat-transfer coefficient yields

$$h = 3600\ \gamma_g v_g c_p \frac{(t_{g,D} - t_s)}{(t_s - t_d)} \qquad (2)$$

The data obtained by this method were correlated in terms of $Nu/Pr^{1/3}$ against Re_s. The physical properties of air were evaluated at the local surface temperature. The results obtained at station C are shown in figure 6, together with theoretical values from references 4, 9, and 15. The data of figure 6(a) were obtained at an airspeed of 275 miles per hour, an angle of attack of 0°, and a gas-flow rate of 91.4 pounds per hour per foot span. The extent of laminar flow is rather limited; most of the heated surface is in the transition region from laminar to turbulent flow. The point corresponding to the end of the transition region and the beginning of fully developed turbulent flow is obtained at approximately $Re_s = 1.1 \times 10^6$. For this point, the experimental value of convective heat-transfer coefficient is about 20 percent lower than for a solid flat plate (ref. 14), 13 percent lower than the value obtained from the

theory of reference 9, and about the same as that obtained from reference 4. Similar results are shown in figures 6(b) to (d) for other values of gas flow, angle of attack, and airspeed. In general, the experimental heat-transfer coefficients of figure 6 for fully developed turbulent flow are 20 to 30 percent lower than the theoretical values for a solid flat plate, while for the same conditions the theories of references 9 and 4 predict heat-transfer coefficients which are 10 to 15 and 20 to 25 percent lower, respectively, than for a solid flat plate.

Comparison of figures 6(a) and (b) shows that an increase in gas-flow rate at constant airspeed results in transition to turbulent flow at a lower Reynolds number. Similarly, decreasing the airspeed with constant gas-flow rate has the same effect of moving the transition region forward (figs. 6(c) and (d)). The movement of the transition region may be correlated by plotting a transition-region Reynolds number obtained from figure 6 against the corresponding local gas- to free-stream-velocity ratio. The Reynolds number at which transition begins or ends is difficult to determine precisely; instead, the value of Reynolds number plotted in figure 7 was obtained from figure 6 for an arbitrary value of $Nu/Pr^{1/3} = 400$. It is shown in figure 7 that the transition region moves forward as the gas- to air-stream-velocity ratio increases. In wet air, the presence of a water film on the leading-edge region may cause transition at a slightly lower Reynolds number than shown in figures 6 and 7.

Airfoil Drag in Icing

The investigation of drag increase due to ice accretions was limited to an airspeed of 275 miles per hour, a datum air temperature of 20° to 25° F, a liquid-water content of 0.5 to 1.0 gram per cubic meter, and angles of attack of 2°, 4°, and 6°. Since the airfoil tested would normally be used on an aircraft having a much higher maximum airspeed than that of the icing tunnel, the effect of large rates of water catch (typical of high-speed operation in clouds of normal water content) was investigated by taking data at the lower airspeed (275 mph) and a high liquid-water content, as suggested in reference 15.

The typical chordwise and spanwise variation of water catch on the airfoil is illustrated by figure 8, where the local impingement efficiency is plotted against surface distance at three spanwise stations for an airspeed of 275 miles per hour, an angle of attack of 2°, a liquid-water content of 0.5 gram per cubic meter, and a mean effective droplet size of 11.5 microns. The results shown were calculated from unpublished wind-tunnel water-droplet impingement data obtained by means of water droplets carrying dye in solution.

The maximum water-collection rate is at about 1/2-percent s/c on the lower surface of the airfoil. On the upper surface, little water impinges beyond 1-percent s/c, and none beyond 5-percent s/c. On the lower surface, most of the water catch is deposited on the heated area. The amount of water impinging beyond the heated area on the lower surface is a relatively small part of the total water catch; because of its location, this water probably does not impose a serious drag penalty (ref. 15). Although the airfoil thickness in inches decreases from root to tip, the total water catch is essentially constant for the three chordwise stations, partly because of the greater collection efficiency of the small-chord stations. In addition, the airfoil pressure distribution showed an increase in effective angle of attack from root to tip, which would also tend to increase the local water catch.

The growth of a rime-ice formation on the unheated airfoil at a datum air temperature of 25° F and the conditions of figure 8 is shown in figure 9(a) to (c). The ice catch on the airfoil consists of the primary formation in the stagnation region, which is building forward into the air stream, and a much lighter secondary formation on the aft part of the porous area. As the icing time increases, the leading-edge ice formation increases in size and becomes more irregular. Aft of the impingement zone, light frost may be seen in areas where the afterbody heating was inadequate. The ice formation at a higher angle of attack (6°) is shown in figure 9(d). The main ice formation at an angle of attack of 6° is farther back on the lower surface than occurred at an angle of attack of 2°, and practically no water is caught on the upper surface.

Typical glaze-ice formations may be seen in figure 10 for angles of attack of 2° and 6°, an airspeed of 275 miles per hour, a datum air temperature of 25° F, and a liquid-water content of 0.85 gram per cubic meter. The cup-shaped ice formation is characteristic of a swept airfoil in glaze icing (ref. 15) and presents a more serious drag problem than the streamlined rime ice (fig. 9). At a datum air temperature of 25° F, glaze ice usually formed at the higher water content (0.85 g/cu m), and rime ice at the lower water content (0.5 g/cu m).

The drag increase with rime-ice formation is shown in figure 11(a) for the three rake stations and the same conditions as for figures 9(a) to (c): airspeed, 275 miles per hour; datum air temperature, 25° F; angle of attack, 2°; and liquid-water content, 0.5 gram per cubic meter. The points at zero icing time for stations A and C were obtained from the previous dry-air survey. The drag coefficient in dry air (zero icing time) increases from stations A to C because of the spanwise increase in effective angle of attack which is associated with the large angle of leading-edge sweepback. The drag at station B increases from 0.0066 to 0.0106 (60 percent) for 10 minutes icing. The greatest increase in drag takes place during the first 6 minutes of icing, after which the increase is more gradual. The increase in drag for a given icing time is greatest

at the smallest chord, as shown by the following example: For 10 minutes icing time, the drag coefficient increase at stations A, B, and C is 27, 60, and 80 percent, respectively. Examination of the water impingement curves (fig. 8) and of the icing photographs (figs. 9 and 10) shows that the size of the ice formation is nearly uniform spanwise. The ice formation at the smallest chord thus represents the greatest distortion of the original airfoil shape and causes the largest increase in drag coefficient.

Similar drag results are shown in figure 11(b) for the same icing condition as figure 11(a) at an angle of attack of 4°. The drag increase is slightly greater at an angle of attack of 4° than at 2° for this icing condition.

A summary of all drag data taken in icing at station B with the leading-edge section unheated is shown in figure 12. At an angle of attack of 6° and a liquid-water content of 0.5 gram per cubic meter, the drag increases sharply in the first $1\frac{1}{2}$ minutes, but further icing causes only a gradual increase in drag; this result is considerably different from that already shown in figure 11 for angles of attack of 2° and 4°.

The penalties to be expected from operation at higher airspeeds in icing clouds of moderate liquid-water content are approximated by the data obtained at a high liquid-water content (0.85 g/cu m) and an airspeed of 275 miles per hour. For an angle of attack of 2° and a datum air temperature of 25° F, the drag coefficient increases in 10 minutes from 0.0065 to 0.0222 (240 percent); while for the same datum air temperature and icing time and an angle of attack of 6°, the increase is from 0.0097 to 0.0248 (155 percent). The rapid increase in drag is caused by the higher ice-accretion rate and the cup-like glaze-ice formations projecting from the leading edge (fig. 10).

In order to assess the penalties resulting from submarginal operation of the anti-icing system, the drag was determined at station B with the leading edge heated for an airspeed of 275 miles per hour, a datum air temperature of 25° F, an angle of attack of 2°, and a liquid-water content of 0.7 gram per cubic meter. The heating rate was set equal to the requirement for complete evaporation at a liquid-water content of 0.4 gram per cubic meter instead of 0.7 gram per cubic meter. The residual ice which formed on the leading-edge section and behind the porous area on the lower surface may be seen in figure 13. After 9 minutes icing time, spots of ice appeared on the leading edge, plus a thin trace of runback ice at the edge of the porous area. The lower-surface residual-ice formation built up to a fairly large size during 34 minutes of icing, but the leading-edge ice changed little in size or extent because of vibration of the model which caused larger pieces of ice to shed periodically. The increase in drag due to the ice formations shown by figure 13 may be seen in figure 14. For the icing condition of figures 13 and 14, the drag

increase with the leading-edge section unheated would be of the order of 6 percent per minute, or more. The rate of drag increase with submarginal heating shown by figure 14 is about 1.2 percent per minute. Consequently, no serious deterioration in performance should be expected if a protection system designed for normal liquid-water content were exposed to a higher liquid-water content for short periods of time. Where the hot-gas supply is limited and exposure to icing conditions is known to be short, a small accumulation of runback on the lower surface might be permitted in order to reduce heating requirements.

From the icing drag data presented, it may be concluded that some form of icing protection usually will be required when aerodynamic heating is not sufficient and when exposure to icing occurs for extended periods of time; however, small formations of runback ice on the lower surface probably may be tolerated without serious loss in performance.

Anti-Icing Performance

Marginal anti-icing heat requirements. - For large bodies such as airfoils, it is usually desirable to heat only the leading-edge region in order to evaporate all impinging water either within the impingement region or within a prescribed distance beyond the limits of impingement (ref. 1). For the purposes of the present investigation the marginal heating rate was defined as the lowest heating rate which would evaporate all water impinging on the heated area.

Photographs of the icing protection afforded by heating rates $[wc_p(t_{g,i} - t_d)]$ varying from 20,300 to 12,100 Btu per hour per foot span are shown in figure 15 for an airspeed of 275 miles per hour, an angle of attack of 2°, a datum air temperature of 0° F, and a liquid-water content of 0.4 gram per cubic meter. No afterbody heating was employed during the determination of marginal heating rates. Adequate protection is obtained at heating rates of 20,300 and 17,000 Btu per hour per foot span; 17,000 Btu per hour per foot span (fig. 15(b)) was considered the marginal heating rate. The gas-flow rate at this point was 143 pounds per hour per foot span, and the entrance gas temperature was 496° F. The two small spots of ice on the leading edge at the joint between adjacent panels of porous metal are too small to produce a noticeable increase in drag. The light ice formation well aft of the heated area outboard of midspan is a result of frost caused by tunnel air-stream turbulence and supersaturation, plus very light impingement. Several pieces of ice may be seen on the leading edge in figure 15(c) where the heating rate is 14,400 Btu per hour per foot span; in addition, several small pieces of ice have built up at the back edge of the porous area. Leading-edge ice forms first in the region between the root and midspan, probably because the hot gas discharging against the baffle loses heat to the wing structure before entering the critical leading-edge region.

Outboard of midspan, where the gas discharges directly into the leading-edge region, the leading edge is ice free. This result is also shown in figure 15(d), where the heating rate is 12,100 Btu per hour per foot span. Since there is little impingement on the upper surface, no runback or residual ice was observed there.

The variation of marginal heating requirement in Btu per hour per foot span with datum air temperature may be seen in figure 16(a) for inlet gas temperatures of 350° and 500° F, an angle of attack of 2°, and several icing conditions. The marginal heating rate increases almost linearly with decreasing datum air temperature; the requirement approximately doubles between a datum air temperature of 20° and 0° F. Figure 16(a) also indicates that the marginal heating rate increases directly with increasing speed for constant datum air temperature. Varying the model inlet gas temperature from 350° to 500° F had little effect on the marginal heating rate.

In general, a higher heating rate should be associated with higher angles of attack since, as angle of attack is increased from 0°, the extent of impingement on the lower surface becomes much greater, while the flow of hot gas to the lower surface becomes less than that to the upper surface as a result of the change in local surface pressures. The variation of marginal heating rate with angles of attack of 0°, 2°, 5°, and 8° is shown in figure 16(b) for an airspeed of 275 miles per hour, a datum air temperature of 20° F, an inlet gas temperature of 500° F, and a liquid-water content of 0.5 gram per cubic meter. The heating rate at an angle of attack of 8° is approximately 40 percent greater than that for 0°.

For a continuous heating system designed for complete evaporation, an increase in water catch due to increased liquid-water content results in a higher marginal heating rate. Figure 16(c) shows the variation in marginal heating rate with liquid-water content for three combinations of airspeed and angle of attack. In the tunnel a larger droplet size is associated with the higher liquid-water content, resulting in increased airfoil collection efficiency. Consequently, doubling the liquid-water content requires more than twice the heating rate, because the water catch is more than twice as large. Typical photographs of the wing model at the marginal heating rates of figure 16 may be seen in figures 15(b) and 17. For the lower range of angle of attack, droplet size, and liquid-water content, the critical heated area was at the leading-edge stagnation region, from wing root to midspan (figs. 15(b) and 17(a) and (b)). This is the span length for which the hot gas discharged against the baffle at the rear of the D-duct, rather than at the leading edge. Improved performance would be obtained by drilling all the hot-gas outlet holes on the forward side of the delivery tube. For the higher values of angle of attack, liquid-water content, and droplet size, the critical area is aft of the heated area, since in this region there is light impingement, which may be combined with runback from the heated area when heating rates are submarginal.

De-icing characteristics. - Although the porous-skin system was designed as a continuous ice-prevention system, it is of interest to examine the de-icing characteristics as well. If the anti-icing system is manually operated, the air supply ordinarily would not be turned on until an ice accretion is observed. In the de-icing tests, ice was allowed to build up on the unheated airfoil for 5 to 10 minutes; the heating rate was then established at the marginal level previously determined. The tests were made at an airspeed of 275 miles per hour and an angle of attack of 4°. After 10 minutes of icing at a datum air temperature of 25° F and a liquid-water content of 0.8 gram per cubic meter, the resultant ice formation was removed in less than 1 minute. After 5 minutes of icing at a datum air temperature of 0° F and a liquid-water content of 0.5 gram per cubic meter, about $1\frac{1}{2}$ minutes was required to remove the ice formation. The de-icing time would be much shorter if the hot-gas supply line were either shortened or preheated during the heat-off or icing period.

Variation of local gas-flow rates. - The chordwise variation of local gas-flow rates for the marginal heating rate is plotted in figure 18 for three spanwise stations and several combinations of airspeed, angle of attack, datum air temperature, gas-flow rate, and gas temperature. The gas-flow rate at an angle of attack of 2° (fig. 18(a) to (d)) is maximum on the upper surface about 4 inches from the zero chord point, and is minimum on the lower surface about 1/2 to 1 inch from zero chord, primarily because of the chordwise variation of external pressure around the airfoil. The local flow rate generally increases slightly toward the tip of the wing because of decreasing pressure on the upper surface. The gas-flow rate is nearly constant spanwise, however, since the heated area decreases slightly in chordwise extent toward the tip.

The flow distribution tends to become more uniform as the duct pressure and gas-flow rate are increased, as shown by the following comparison of figures 18(a) and (b): For station B, the ratio of maximum local flow rate to minimum flow rate is 2.5 for a gas-flow rate of 82.5 pounds per hour per foot span and 1.9 for 134 pounds per hour per foot span. Consequently, for a given total flow rate, it is desirable to use as large a pressure drop as possible, within the structural limitations of the leading-edge section, by decreasing the porosity of the metal.

The effect of angle of attack on gas-flow distribution may be seen by comparing figures 18(d), (e), (f), and (g). At an angle of attack of 0°, the flow distribution is symmetrical with respect to the zero chord line and is minimum at the zero chord line (stagnation). At an angle of attack of 5° (fig. 18(f)), the curves are similar to those for 2° except that a much larger proportion of the gas is delivered to the upper surface because of the decrease in local pressure on the upper surface. At an angle of attack of 8° (fig. 18(g)), the effect is even more pronounced.

However, since practically no water impinges on the upper surface at the higher angles of attack, most of the gas flow through the upper surface is wasted.

For a vertical fin which normally operates at an angle of attack of 0°, the arrangement of equal heatable areas on the upper and lower surfaces is satisfactory. If the airfoil is used as a lifting surface, it might normally operate at an angle of attack of 2° for the climb and cruise conditions, and at higher angles of attack for maneuvers, low speed, landing, and take-off. For positive angles of attack, a better distribution of hot gas would be obtained if the chordwise extent of upper-surface porous area was less than that of the lower surface. Unpublished data showed that for an angle of attack of 2°, the rear half of the upper-surface porous area could be sealed without obtaining any residual ice or runback. Accordingly, the data of figures 18(a), (f), and (g) were reevaluated with the assumption that the chordwise distance heated on the upper surface is reduced to one-half the distance on the lower surface ($s_U = 0.5\ s_L$). The saving in total gas flow (shown in fig. 19) varies from 31 to 42 percent for the range of angle of attack from 2° to 8°.

Surface and internal temperatures. - Typical surface temperatures in icing conditions with marginal heating rates are shown in figures 20 and 21. The spanwise and chordwise distributions of surface temperature are shown in figure 20 for an airspeed of 275 miles per hour, an angle of attack of 2°, a datum air temperature of 20° F, a liquid-water content of 0.5 gram per cubic meter, a gas-flow rate of 82.5 pounds per hour per foot span, and an inlet gas temperature of 481° F. The temperature of the porous skin is rather high, in order to obtain complete evaporation of the water caught in the heated area. Beyond the heated area the temperature drops sharply at first, then becomes asymptotic to the datum air temperature. From this it may be seen that the protected area generally is greater than the heating limit defined by the baffle and the porous area because of carry-over of heat in the boundary layer and of chordwise conduction of heat. The average surface temperature decreases with increasing span (increased distance from hot-gas inlet) as a result of the spanwise drop in gas temperature.

The variation of surface-temperature profiles with angle of attack, airspeed, inlet gas temperature, and datum air temperature may be seen in figure 21 for station C. At an angle of attack of 0° (fig. 21(a)) the temperature distribution is nearly symmetrical, with the minimum temperature at the zero chord point. At an angle of attack of 2° (fig. 20) the surface temperature at station C is highest on the upper surface, where impingement is negligible and the local gas-flow rate is maximum. The minimum temperature is on the lower surface near the zero chord point, where the local impingement rate is near maximum and the local gas-flow rate is minimum; aft of this point the temperature increases

until the limit of heated area is reached. The temperature profiles at angles of attack of 5° and 8° (fig. 21(a)) are similar to that for an angle of attack of 2°, except that the variation in surface temperature between upper and lower surface is greater because the gas flow through the upper surface increases with increased angle of attack. The temperature profiles shown in figure 21(b) for station C at an angle of attack of 2° and various icing conditions are similar to the temperature profile of figure 20, except for the reduced temperature level in the case of lower gas temperature or airspeed, and the higher temperature level in the case of lower datum air temperature.

The internal gas and structural temperatures are plotted as a function of spanwise distance in figure 22. The highest temperature is that of the hot gas in the delivery tube. The rib temperatures are at the same level as the D-duct temperatures since the ribs are exposed directly to the hot gas. The baffle temperature is midway between the D-duct gas temperature and the temperature of the air chamber between the spar and the baffle. The point of attachment between the baffle and spar gave the highest spar temperature, while the main part of the spar was considerably lower in temperature, usually less than 100° F. No particular structural problems should arise from the temperatures encountered since the members in contact with the hot gas (porous skin, ribs, and baffle) were of stainless steel, while the temperatures of the aluminum components (solid skin and main spar) were comparatively low.

From figure 22 it is evident that improved system performance could be obtained by reducing the spanwise temperature loss and the temperature drop between the delivery tube and the D-duct. The large temperature difference between the delivery tube and the D-duct is a result of heat loss by conduction to the ribs, baffle, spar, and solid skin. This heat loss could be reduced either by using a lower entrance gas temperature (and higher gas-flow rate) or by insulating the ribs, baffle, and point of attachment of the leading-edge section to the afterbody. The heat saving due to the insulation would, of course, be offset somewhat by the increased weight. The temperature in the delivery tube drops rapidly spanwise because of the lower temperature of the surrounding gas in the D-duct. If any appreciable length of span must be protected, a full-span delivery tube having a layer of insulation on the outside of the tube should be provided to minimize the spanwise temperature drop and ensure that the tip areas are protected.

SUMMARY OF RESULTS

The results of an investigation of a porous gas-heated leading-edge section for icing protection of a delta wing may be summarized as follows:

1. Satisfactory anti-icing protection was obtained at all conditions investigated. A gas-flow rate of 143 pounds per hour per foot span with an entrance gas temperature of 496° F was sufficient for protection at the following condition: airspeed, 275 miles per hour; datum air temperature, 0° F; angle of attack, 2°; and liquid-water content, 0.4 gram per cubic meter.

2. Ice formation on the unheated leading edge, which may occur prior to activation of the heating system, was removed in 1 to $1\frac{1}{2}$ minutes by a hot-gas-flow rate that would be sufficient for normal anti-icing.

3. A full-span insulated hot-gas delivery tube should be provided to minimize the spanwise gas-temperature loss.

4. For positive angles of attack, a saving in total gas-flow rate for anti-icing of 31 to 42 percent may be obtained with no loss in anti-icing effectiveness by sealing half the upper-surface porous area.

5. Gas flow through the porous leading-edge section had no appreciable effect on airfoil pressure distribution. Sealing the porous area did not affect the airfoil pressure distribution.

6. Gas flow through the porous area sufficient to provide icing protection caused a slight increase in airfoil drag (5-percent average) in most cases. Sealing the porous area did not change the airfoil drag.

7. The section drag coefficient of the unheated airfoil increased from 0.0066 to 0.0106 (60 percent) in 10 minutes of icing at moderate liquid-water content. A heavy glaze-ice formation, formed at a high liquid-water content, caused an increase in section drag coefficient from 0.0065 to 0.0222 (240 percent) in 10 minutes.

8. The extent of laminar flow in dry air with gas flow was small; most of the heated area was in the transition region from laminar to turbulent flow. The transition region moved forward as the ratio of gas velocity through the porous surface to free-stream velocity increased.

9. Experimental convective heat-transfer coefficients in dry air and turbulent flow were approximately 20 to 30 percent lower than the theoretical values for a solid surface, while the theories of Friedman and Mickley predict for the same conditions a reduction of 10 to 15 and 20 to 25 percent, respectively.

Lewis Flight Propulsion Laboratory
National Advisory Committee for Aeronautics
Cleveland, Ohio, September 9, 1954

APPENDIX - SYMBOLS

The following symbols are used in this report:

C_D section drag coefficient, dimensionless

C_p pressure coefficient, dimensionless, $(p_l - p_0)/q_0$

c airfoil chord length measured parallel to air stream, ft

c_p specific heat of air at constant pressure, Btu/(lb)(°F)

g acceleration due to gravity, ft/sec^2

h convective heat-transfer coefficient, Btu/(hr)(sq ft)(°F)

k thermal conductivity of air, Btu/(hr)(ft)(°F)

Nu Nusselt number, dimensionless, hs/k

Pr Prandtl number, dimensionless, $3600gc_p\mu/k$

p static pressure, lb/sq ft

q dynamic pressure, $(1/2)\rho v^2$, lb/sq ft

Re_s Reynolds number based on surface distance, dimensionless, $\rho vs/\mu$

s distance from zero chord measured along airfoil surface parallel to air stream, ft

T temperature, °R

t_d datum air temperature, °F

$t_{g,D}$ duct gas temperature, °F

$t_{g,i}$ gas temperature at delivery-tube inlet, °F

t_s temperature at surface of porous metal, °F

v velocity, ft/sec

w gas-flow rate, lb/(hr)(ft span measured perpendicular to air stream)

x distance from zero chord point measured along chord line parallel to air stream, ft

y droplet trajectory ordinate, ft

α airfoil angle of attack, deg

β local impingement efficiency, dimensionless, $\beta = dy_0/ds$

γ specific weight, lb/cu ft

ρ density, lb-sec^2/ft^4

μ viscosity, lb-sec/sq ft

τ thickness of porous metal, ft

Subscripts:

D duct

g gas

L lower surface

l local conditions at airfoil surface

U upper surface

0 free-stream conditions

1 upstream

2 downstream

REFERENCES

1. Gelder, Thomas F., Lewis, James P., and Koutz, Stanley L.: Icing Protection for a Turbojet Transport Airplane: Heating Requirements, Methods of Protection, and Performance Penalties. NACA TN 2866, 1953.

2. Lewis, James P., and Bowden, Dean T.: Preliminary Investigation of Cyclic De-Icing of an Airfoil Using an External Electric Heater. NACA RM E51J30, 1952.

3. Gray, Vernon H., and Bowden, Dean T.: Comparison of Several Methods of Cyclic De-Icing of a Gas-Heated Airfoil. NACA RM E53C27, 1953.

4. Mickley, H. S., Ross, R. C., Squyers, A. L., and Stewart, W. E.: Heat, Mass, and Momentum Transfer for Flow over a Flat Plate with Blowing or Suction. NACA TN 3208, 1954.

5. Hudson, Victor, Wills, Ross C., and Weiner, Frederick R.: Project Summit Final Report - Radome Thermal Anti-Icing System Development. Rep. No. ZJ-004, San Diego Div., Consolidated Vultee Corp., Aug. 29, 1951. (Contract BuAer NOa(s)-51-209(c).)

6. Schafer, Louis J., Jr., Bartoo, Edward R., and Richards, Hadley T.: Experimental Investigation of the Heat-Transfer Characteristics of an Air-Cooled Sintered Porous Turbine Blade. NACA RM E51K08, 1952.

7. Broadwell, J. E., and Sherman, P.: Survey of Porous-Wall Heat-Transfer Literature. Eng. Res. Inst., Univ. Michigan, Apr. 1953. (Wright Air Dev. Center, U.S. Air Force Contract AF 18(600)-51, E.O. No. 462 Br-1, Proj. M992-7.)

8. Eckert, E. R. G., and Livingood, John N. B.: Comparison of Convection-, Transpiration-, and Film-Cooling Methods with Air as Coolant. NACA TN 3010, 1953.

9. Friedman, Joseph: A Theoretical and Experimental Investigation of Rocket-Motor Sweat Cooling. Jour. Am. Rocket Soc., no. 79, Dec. 1949, pp. 147-154.

10. Eckert, E. R. G., and Livingood, John N. B.: Method for Calculation of Laminar Heat Transfer in Air Flow Around Cylinders of Arbitrary Cross Section (Including Large Temperature Differences and Transpiration Cooling). NACA Rep. 1118, 1953. (Supersedes NACA TN 2733.)

11. Hudson, Victor, Weiner, Frederick R., Wills, Ross C., and Hine, Ernest: Progress Report - Anti-Icing Systems Design and Development, Jan.-June, 1952, YF-102 Airplane. Rep. No. ZJ-8-001, San Diego Div., Consolidated Vultee Corp., Aug. 8, 1952. (Contract AF33(600)5942.)

12. Bartoo, Edward R., Schafer, Louis J., Jr., and Richards, Hadley T.: Experimental Investigation of Coolant-Flow Characteristics of a Sintered Porous Turbine Blade. NACA RM E51K02, 1952.

13. Libby, Paul A., Kaufman, Lawrence, and Harrington, R. Paul: An Experimental Investigation of the Isothermal Laminar Boundary Layer on a Porous Flat Plate. Jour. Aero. Sci., vol. 19, no. 2, Feb. 1952, pp. 127-134.

14. Boelter, L. M. K., Grossman, L. M., Martinelli, R. C., and Morrin, E. H.: An Investigation of Aircraft Heaters. XXIX - Comparison of Several Methods of Calculating Heat Losses from Airfoils. NACA TN 1453, 1948.

15. Gray, Vernon H., and von Glahn, Uwe H.: Effect of Ice and Frost Formations on Drag of NACA 65_1-212 Airfoil for Various Modes of Thermal Ice Protection. NACA TN 2962, 1953.

TABLE I. - LOCATION OF MAIN INSTRUMENTATION

PLANES

Station (see fig. 2)	Instrumentation plane	Distance from tunnel side-wall, in.	Airfoil chord, in.
A	Pressure	19.5	121.1
	Wake survey[a]	20.3	120.8
	Temperature	23.6	114.8
B	Pressure	40.6	85.3
	Wake survey[a]	41.1	83.8
	Temperature	44.8	78.0
C	Pressure	57.8	55.8
	Wake survey[a]	58.4	55.1
	Temperature	62.1	48.3
D	Temperature	76.7	23.0

[a]All wake survey stations located 25-percent chord behind airfoil.

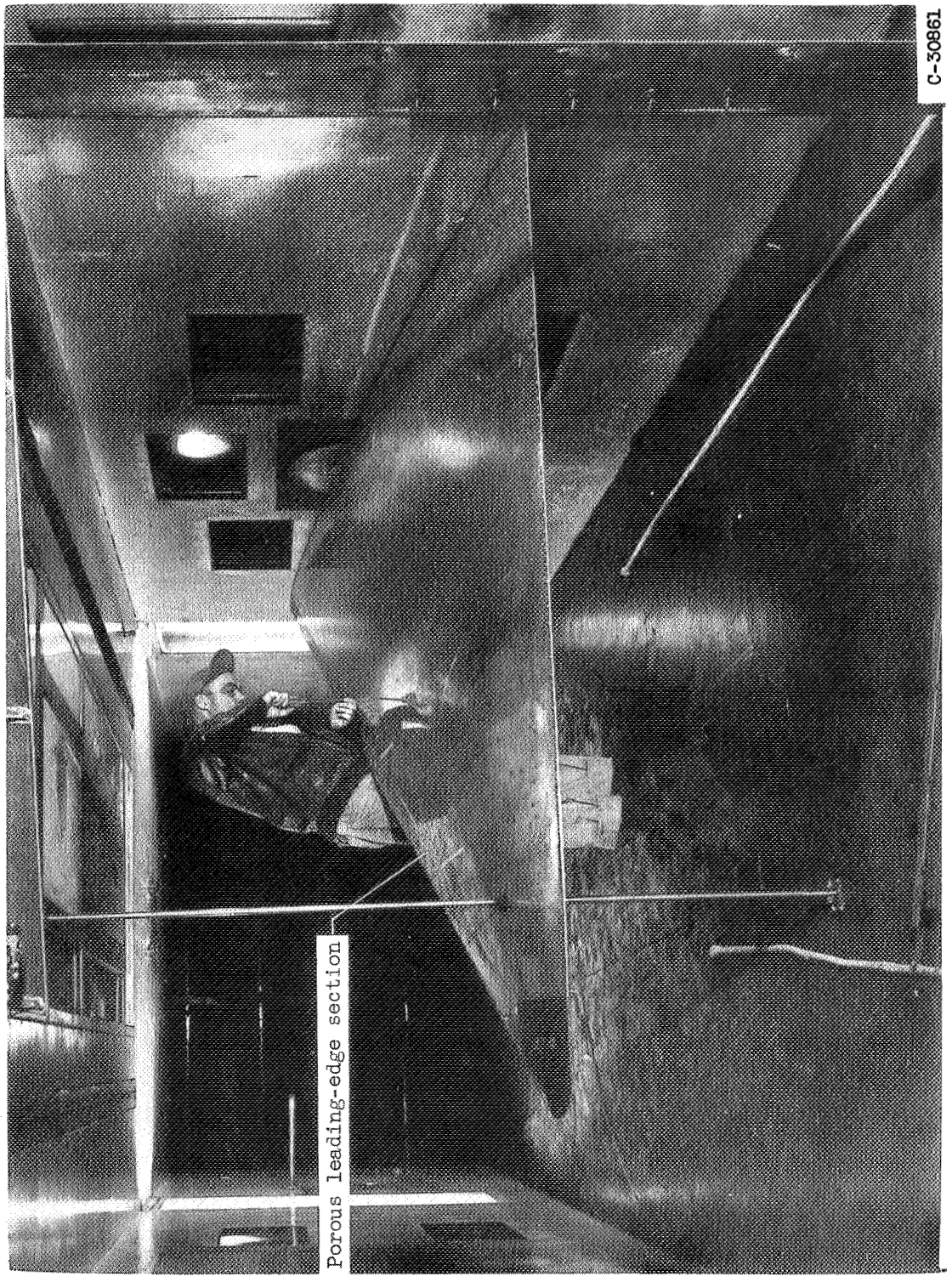

Figure 1. - Installation of model in 6- by 9-foot icing research tunnel.

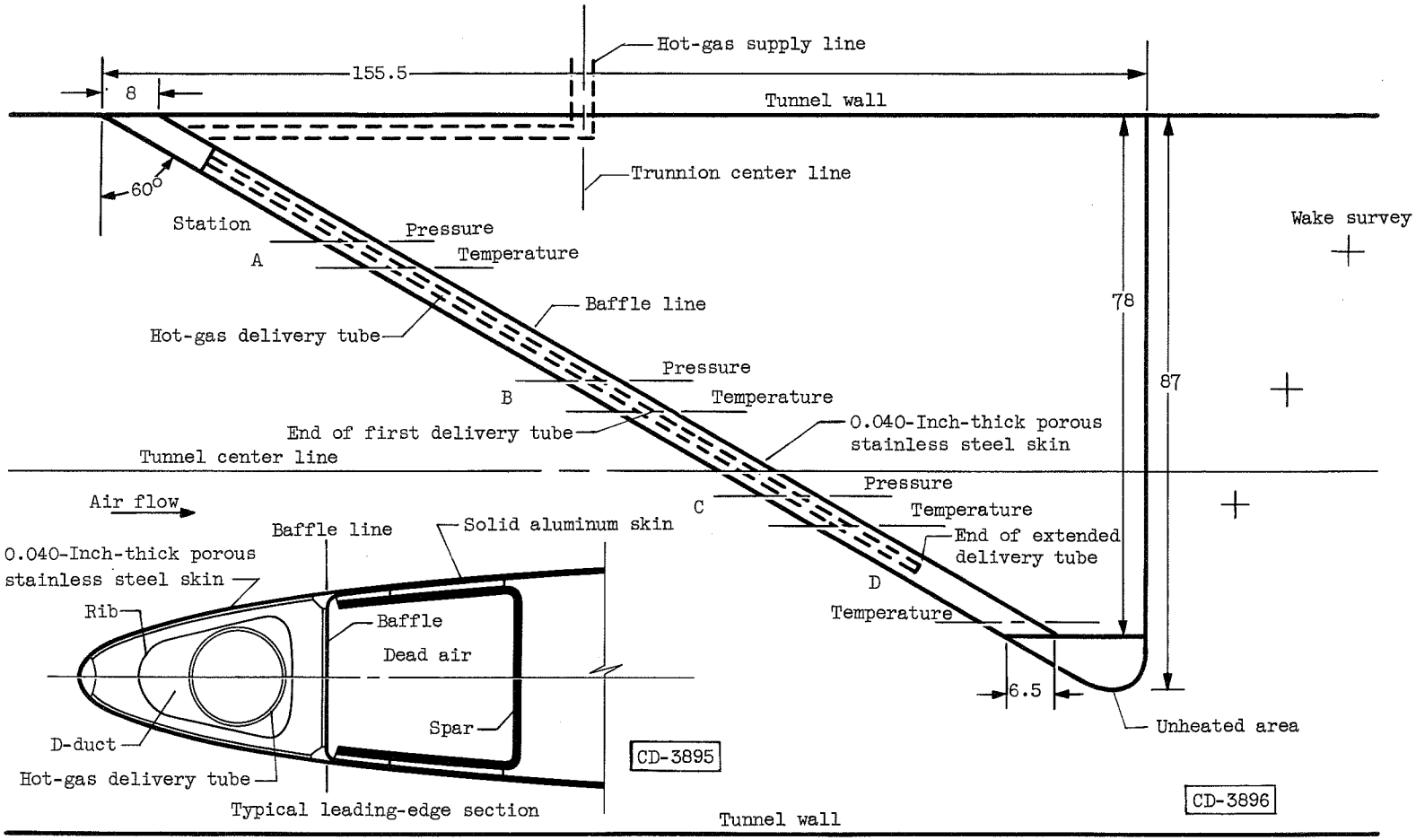

Figure 2. - Sketch of model showing instrumentation stations and leading-edge section. (All dimensions in inches.)

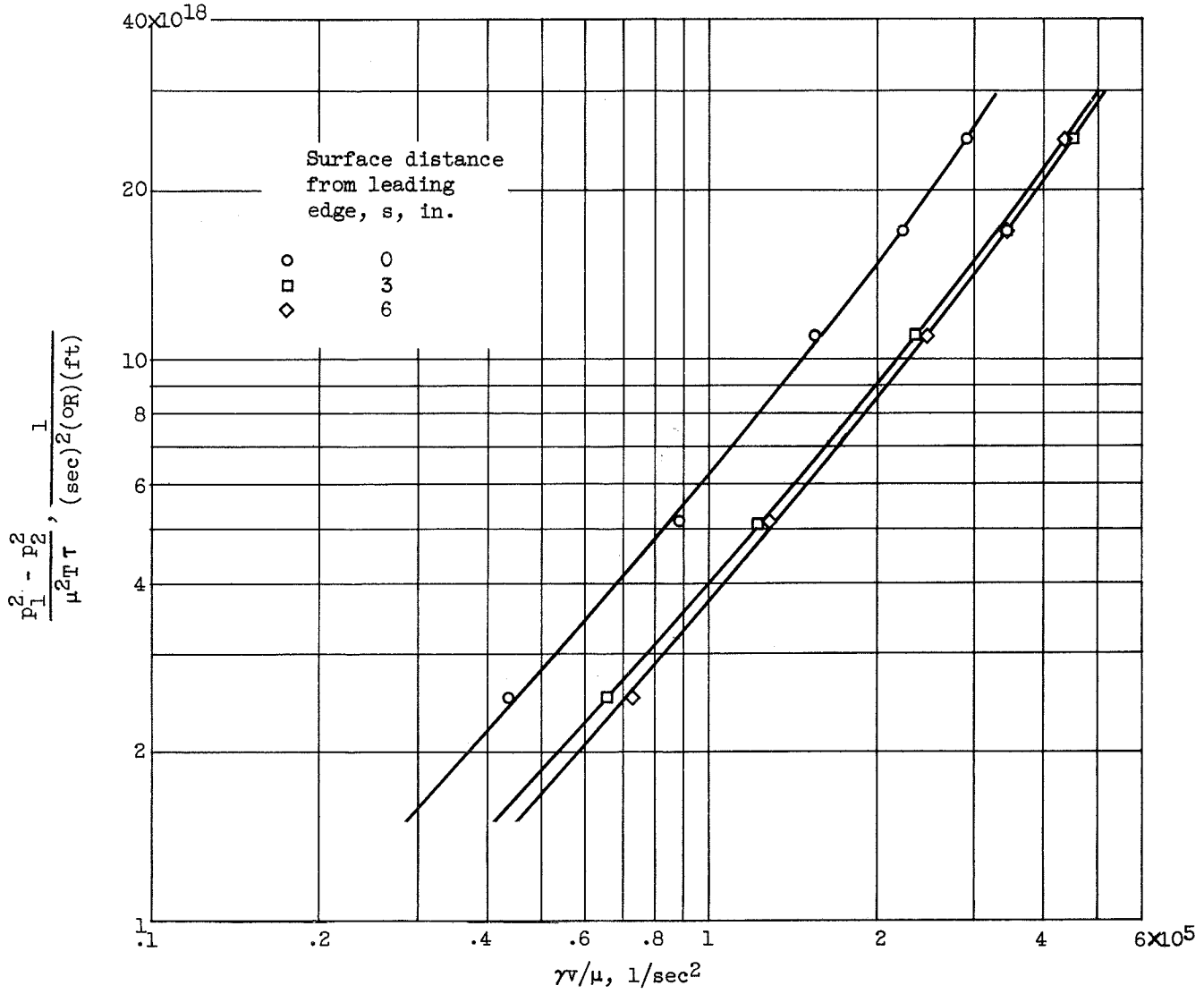

Figure 3. - Flow correlation curves for porous leading-edge section at station A.

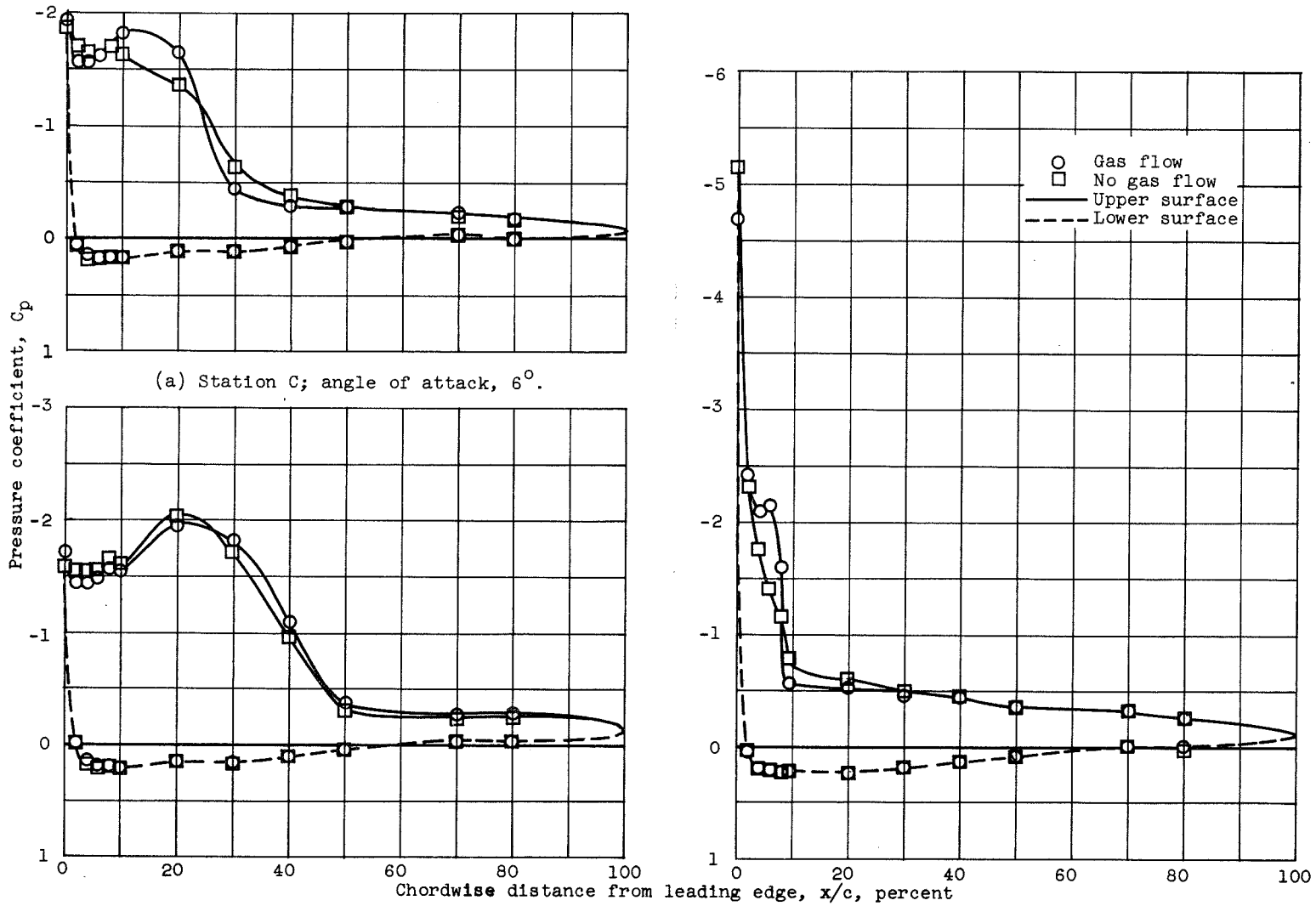

(a) Station C; angle of attack, 6°.

(b) Station C; angle of attack, 8°.

(c) Station B; angle of attack, 8°.

Figure 4. - Airfoil pressure distribution.

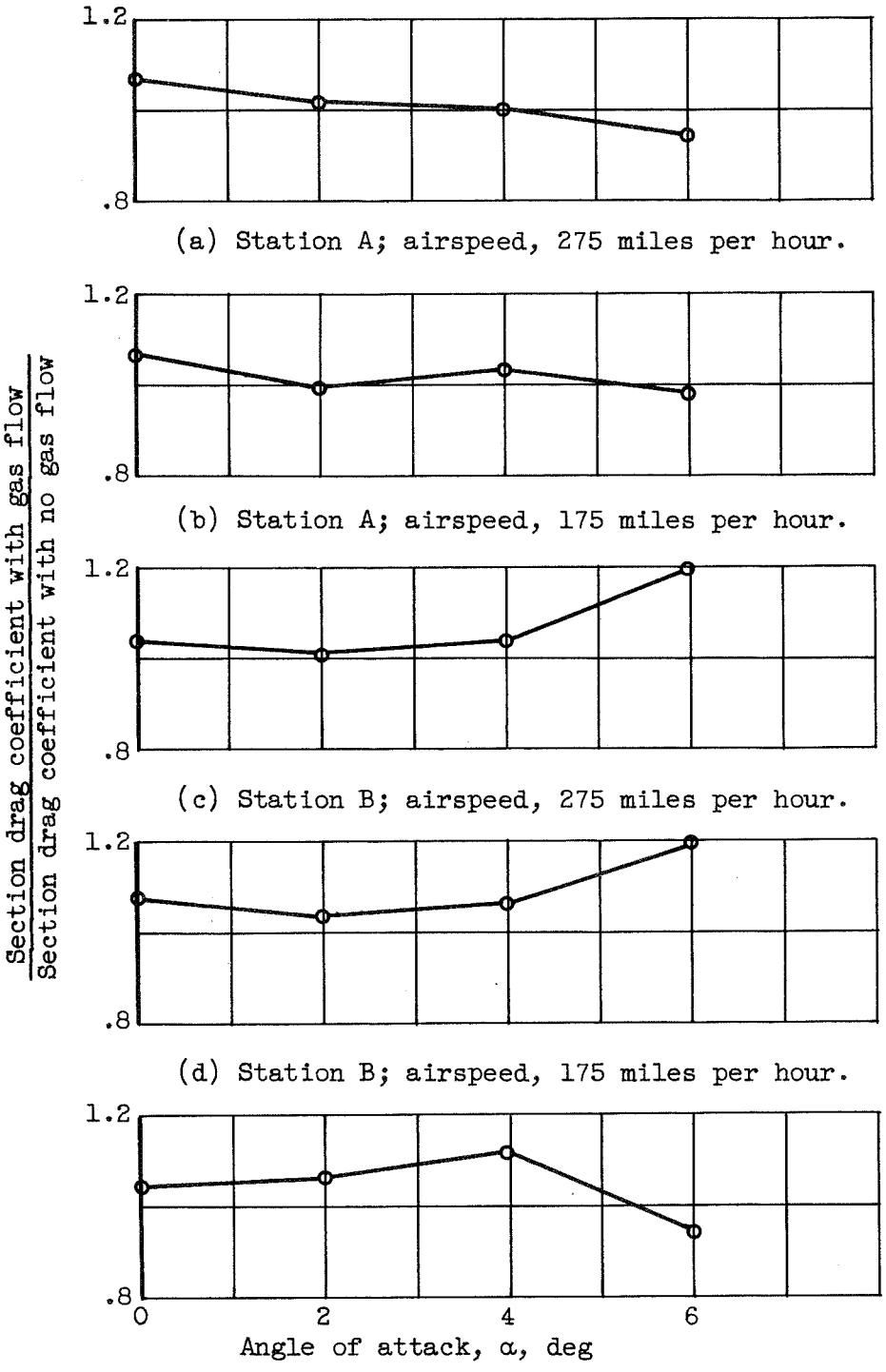

(a) Station A; airspeed, 275 miles per hour.

(b) Station A; airspeed, 175 miles per hour.

(c) Station B; airspeed, 275 miles per hour.

(d) Station B; airspeed, 175 miles per hour.

(e) Station C; airspeed, 275 miles per hour.

Figure 5. - Effect of gas flow through porous area on airfoil drag. Gas-flow rate, 135 pounds per hour per foot span.

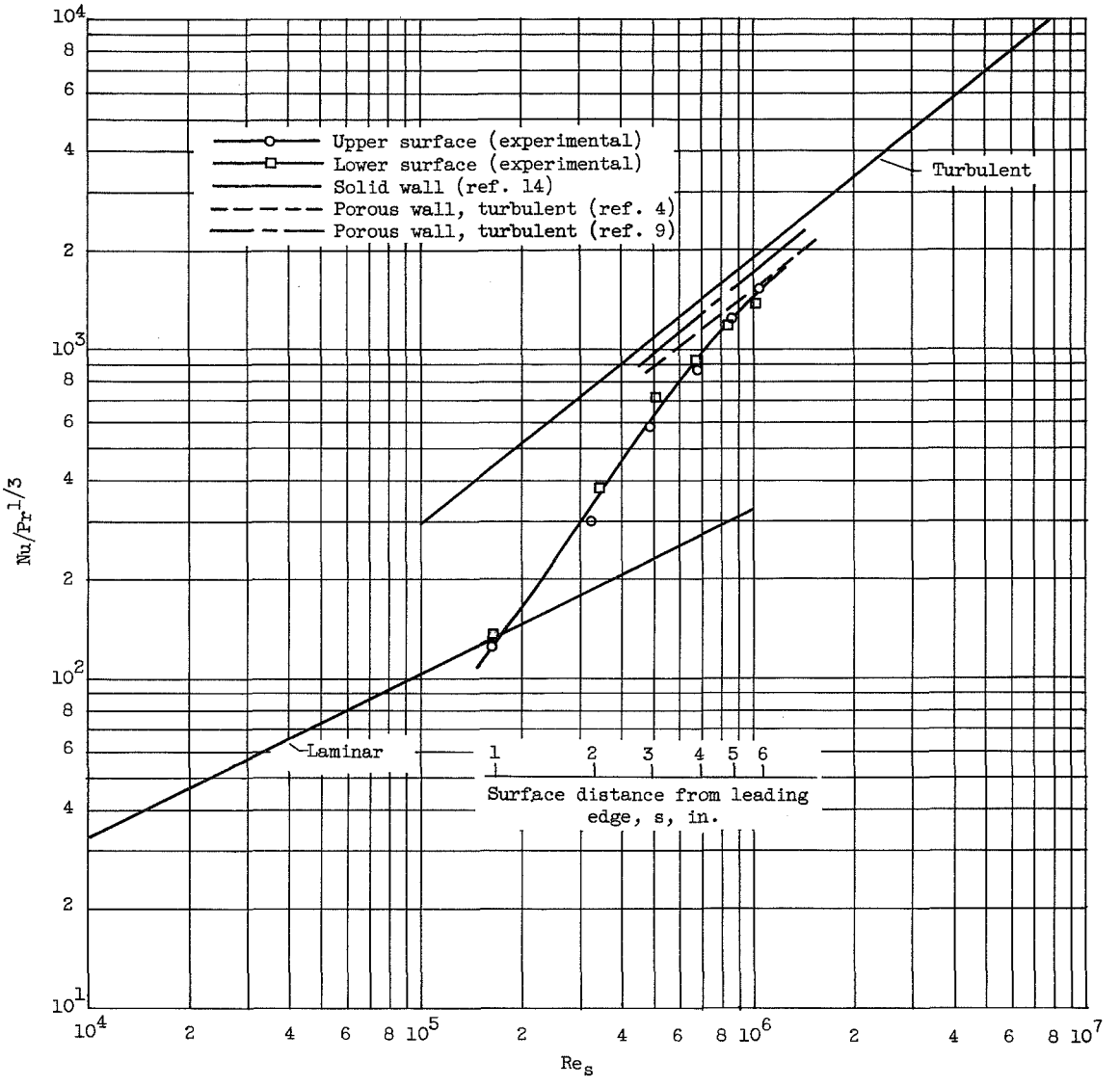
Upper surface (experimental)
Lower surface (experimental)
Solid wall (ref. 14)
Porous wall, turbulent (ref. 4)
Porous wall, turbulent (ref. 9)
Turbulent
Laminar
1 2 3 4 5 6
Surface distance from leading edge, s, in.
Nu/Pr^1/3
Re_s
10^4 8 6 4 2 10^3 8 6 4 2 10^2 8 6 4 2 10^1
10^4 2 4 6 8 10^5 2 4 6 8 10^6 2 4 6 8 10^7

(a) Airspeed, 275 miles per hour; angle of attack, 0°; gas-flow rate, 91.4 pounds per hour per foot span; duct gas temperature, 264° F.

Figure 6. - Correlation of experimental convective heat-transfer coefficients obtained in dry air at station C.

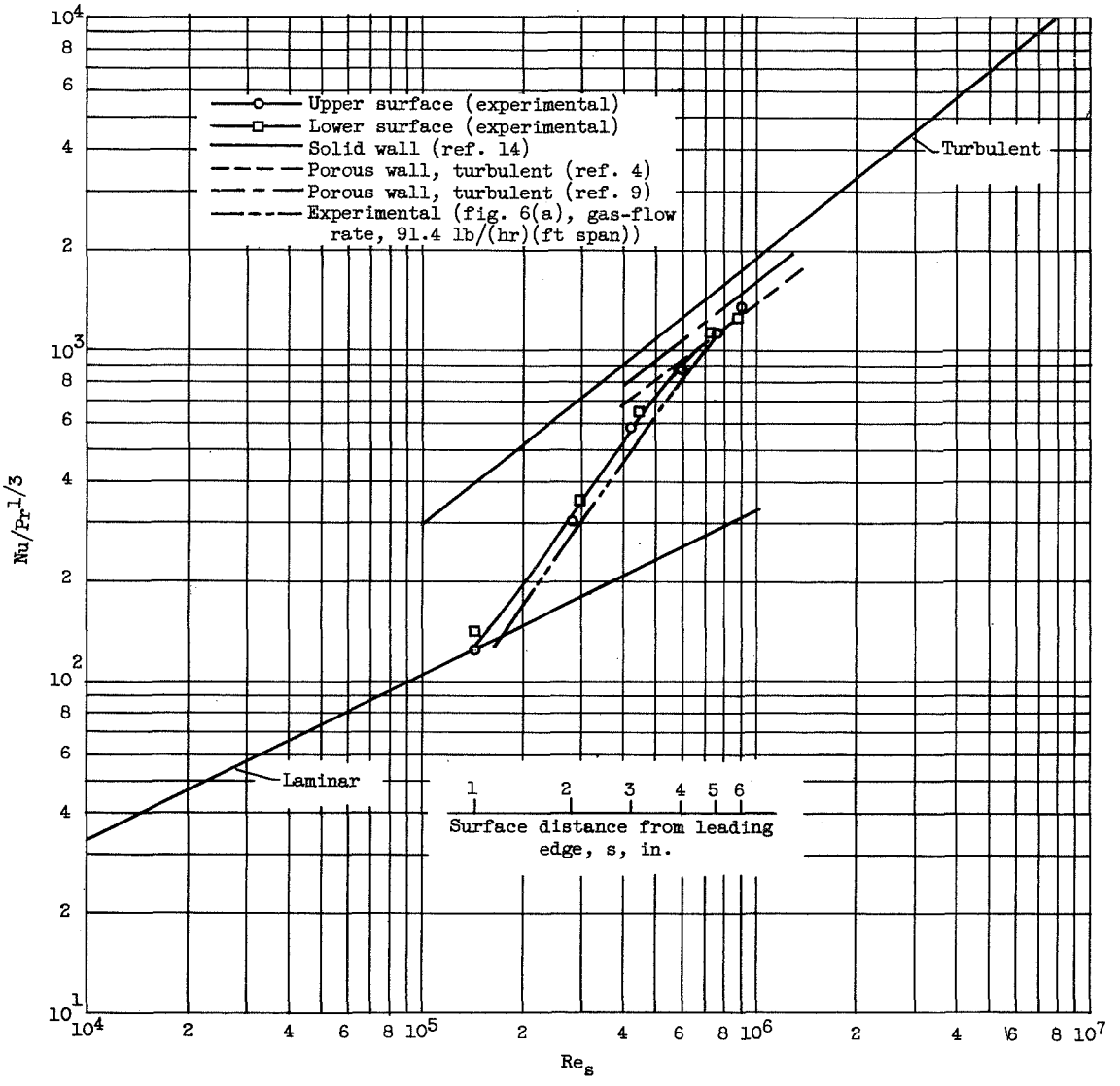
Upper surface (experimental)
Lower surface (experimental)
Solid wall (ref. 14)
Porous wall, turbulent (ref. 4)
Porous wall, turbulent (ref. 9)
Experimental (fig. 6(a), gas-flow rate, 91.4 lb/(hr)(ft span))
Turbulent
Laminar
1 2 3 4 5 6
Surface distance from leading edge, s, in.
Nu/Pr^1/3
Re_s
10^4 8 6 4 2 10^3 8 6 4 2 10^2 8 6 4 2 10^1
10^4 2 4 6 8 10^5 2 4 6 8 10^6 2 4 6 8 10^7

(b) Airspeed, 275 miles per hour; angle of attack, 0°; gas-flow rate, 135 pounds per hour per foot span; duct gas temperature, 318° F.

Figure 6. - Continued. Correlation of experimental convective heat-transfer coefficients obtained in dry air at station C.

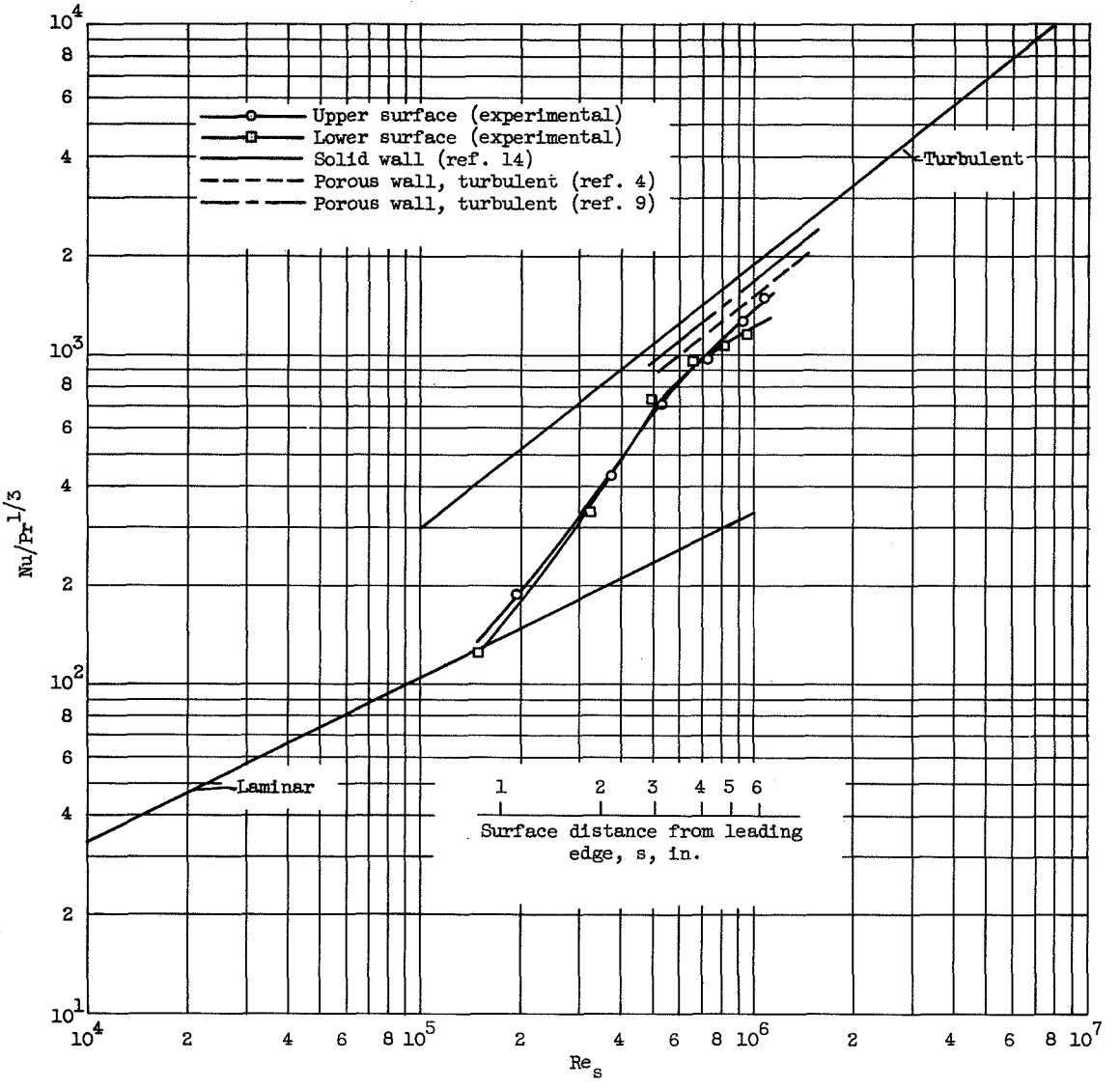
Upper surface (experimental)
Lower surface (experimental)
Solid wall (ref. 14)
Porous wall, turbulent (ref. 4)
Porous wall, turbulent (ref. 9)
Turbulent
Laminar
1 2 3 4 5 6
Surface distance from leading edge, s, in.
Nu/Pr^1/3
Re_s
10^4 8 6 4 2 10^3 8 6 4 2 10^2 8 6 4 2 10^1
10^4 2 4 6 8 10^5 2 4 6 8 10^6 2 4 6 8 10^7

(c) Airspeed, 275 miles per hour; angle of attack, 2°; gas-flow rate, 92.7 pounds per hour per foot span; duct gas temperature, 263° F.

Figure 6. - Continued. Correlation of experimental convective heat-transfer coefficients obtained in dry air at station C.

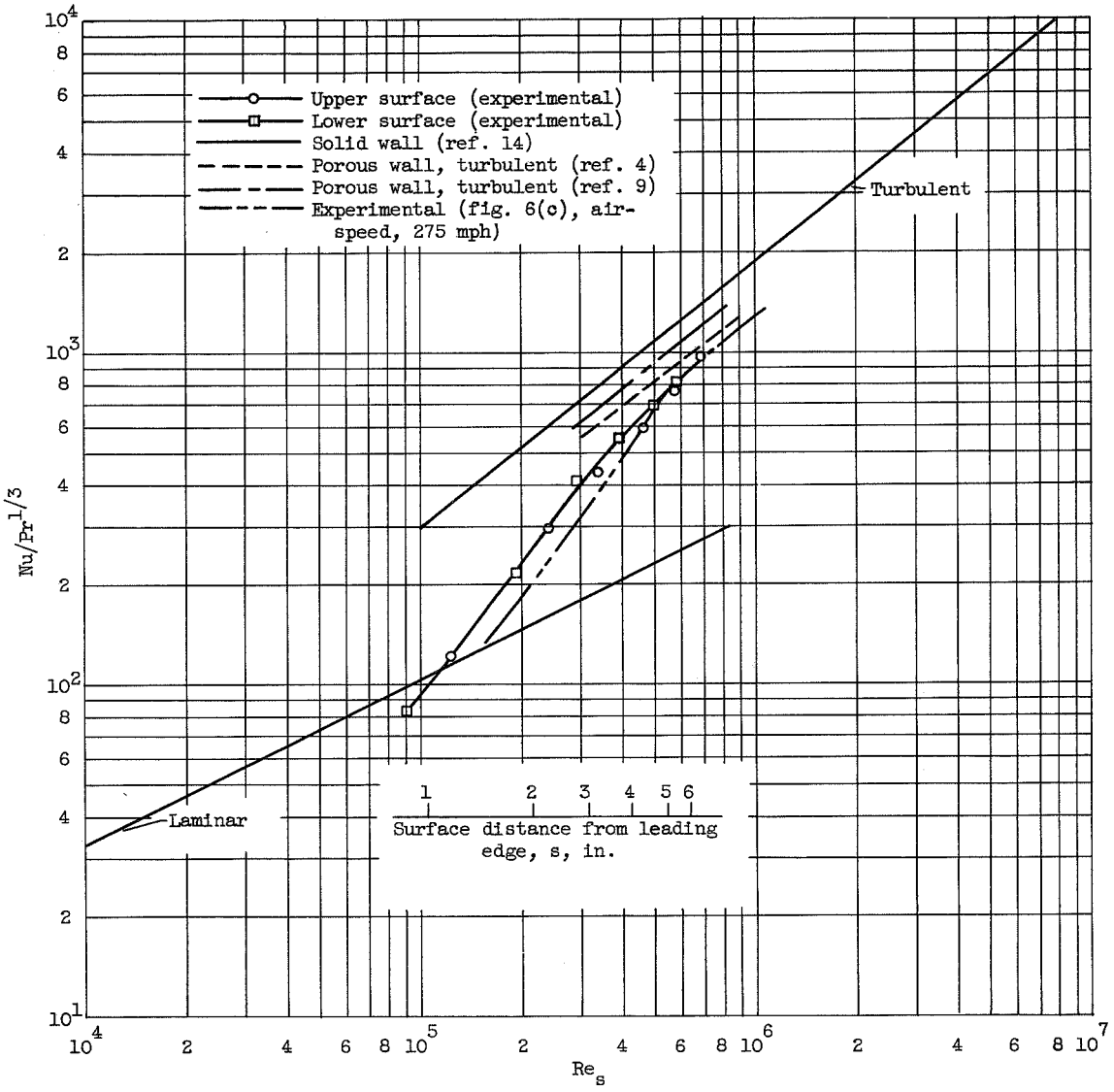
Upper surface (experimental)
Lower surface (experimental)
Solid wall (ref. 14)
Porous wall, turbulent (ref. 4)
Porous wall, turbulent (ref. 9)
Experimental (fig. 6(c), airspeed, 275 mph)
Turbulent
Laminar
1 2 3 4 5 6
Surface distance from leading edge, s, in.
Nu/Pr^1/3
Re_s
10^4 8 6 4 2 10^3 8 6 4 2 10^2 8 6 4 2 10^1
10^4 2 4 6 8 10^5 2 4 6 8 10^6 2 4 6 8 10^7

(d) Airspeed, 175 miles per hour; angle of attack, 2°; gas-flow rate, 92.0 pounds per hour per foot span; duct gas temperature, 287° F.

Figure 6. - Concluded. Correlation of experimental convective heat-transfer coefficients obtained in dry air at station C.

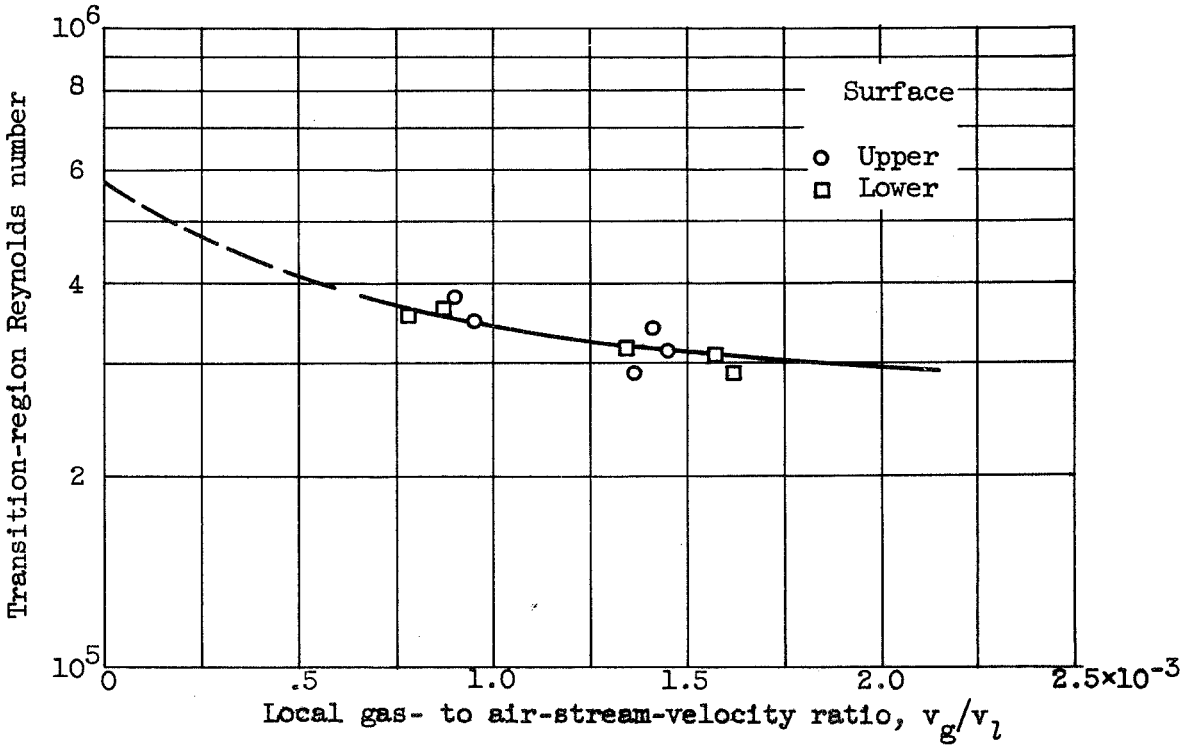

Figure 7. - Forward movement of transition region with increasing gas- to air-stream-velocity ratio.

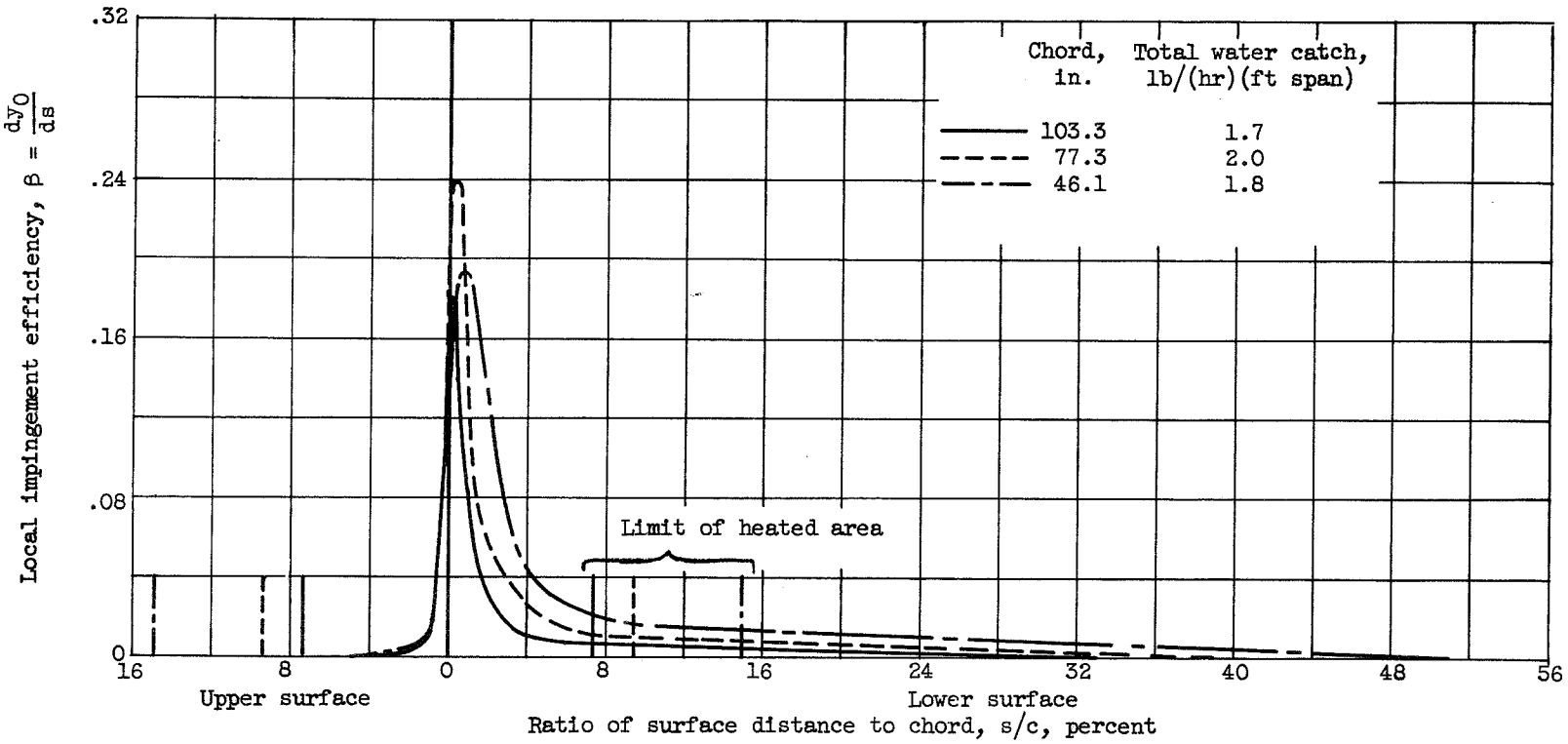

Figure 8. - Chordwise variation of local impingement efficiency for three spanwise stations. Airspeed, 275 miles per hour; angle of attack, 2°; liquid-water content, 0.5 gram per cubic meter; mean effective droplet size, 11.5 microns; maximum droplet size, 28.5 microns.

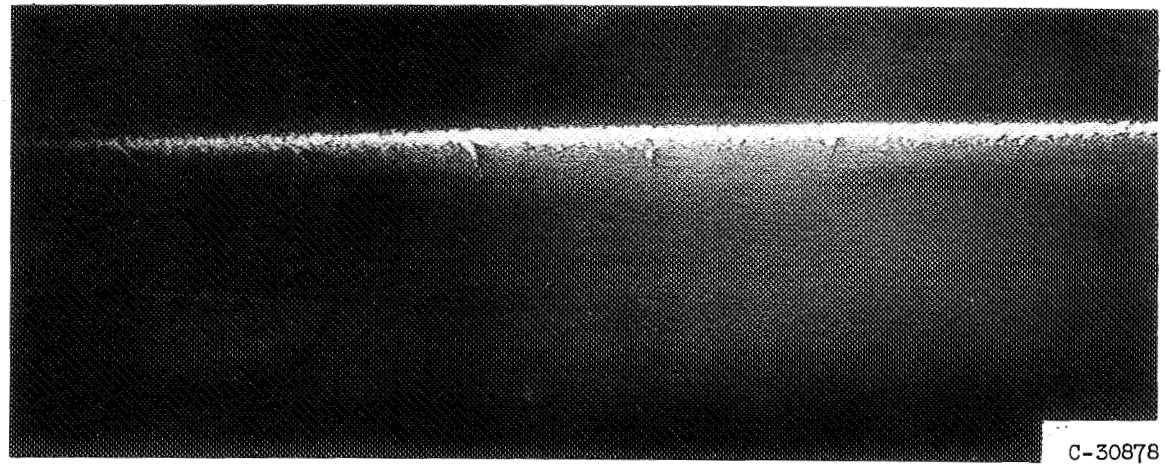

(a) Angle of attack, 2°; icing time, 4 minutes.

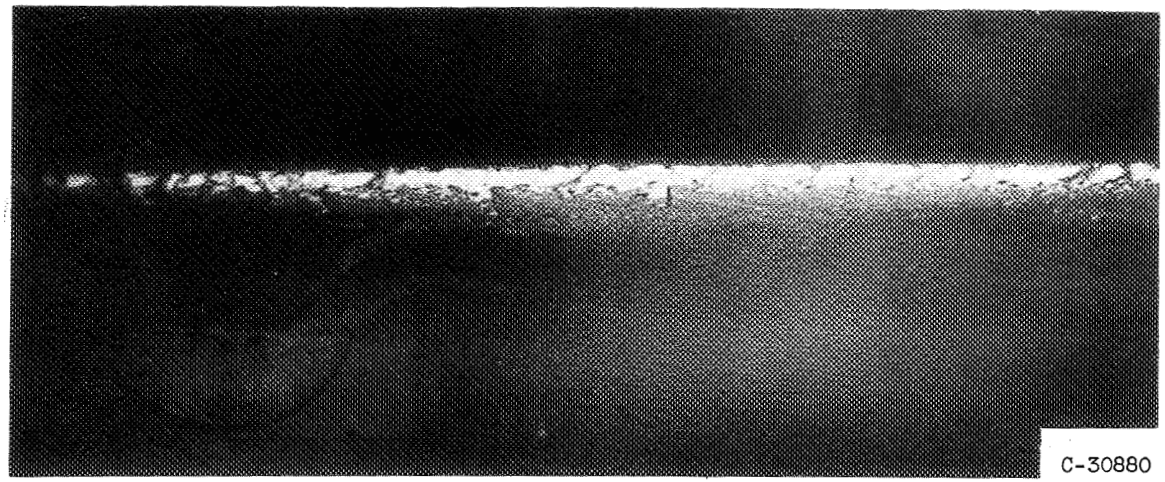

(b) Angle of attack, 2°; icing time, 10 minutes.

Figure 9. - Growth of rime-ice formation on airfoil. Airspeed, 275 miles per hour; datum air temperature, 25° F; liquid-water content, 0.5 gram per cubic meter.

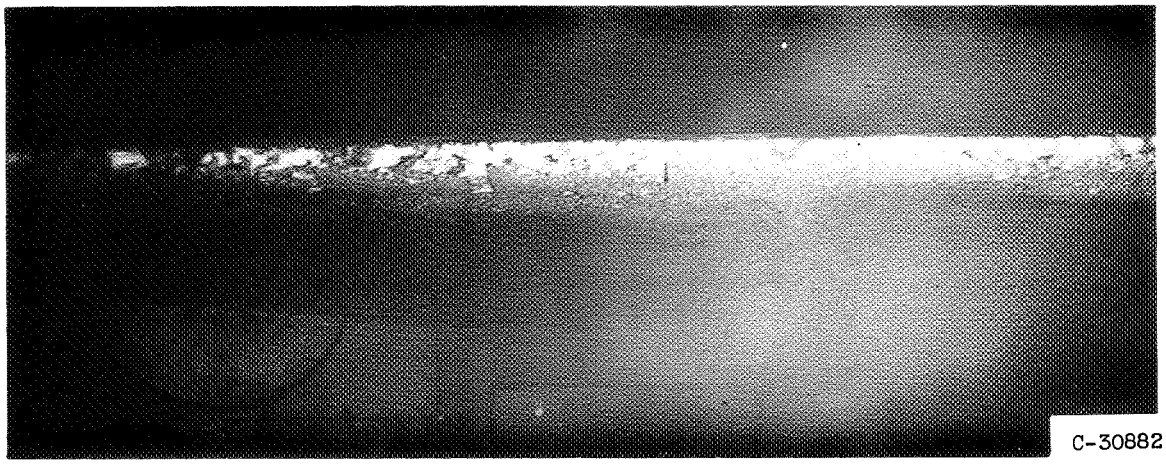

(c) Angle of attack, 2°; icing time, 15 minutes.

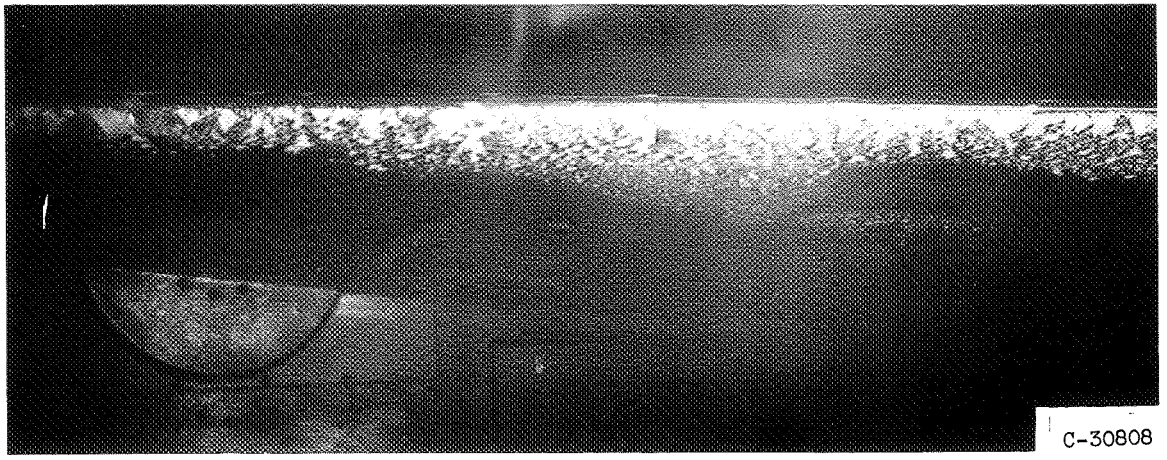

(d) Angle of attack, 6°; icing time, 14 minutes.

Figure 9. - Concluded. Growth of rime-ice formation on airfoil. Airspeed, 275 miles per hour; datum air temperature, 25° F; liquid-water content, 0.5 gram per cubic meter.

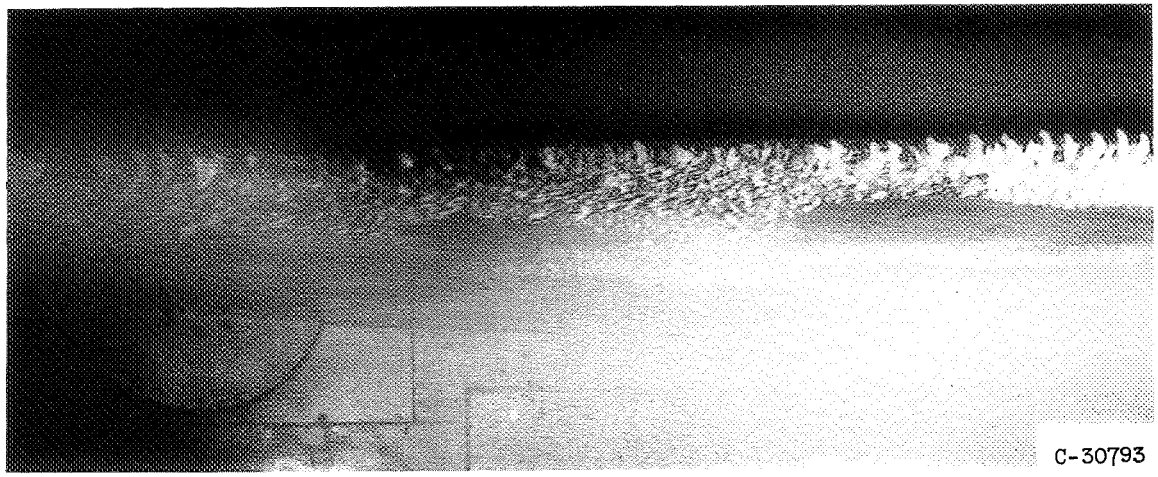

(a) Angle of attack, 2°; icing time, 14 minutes.

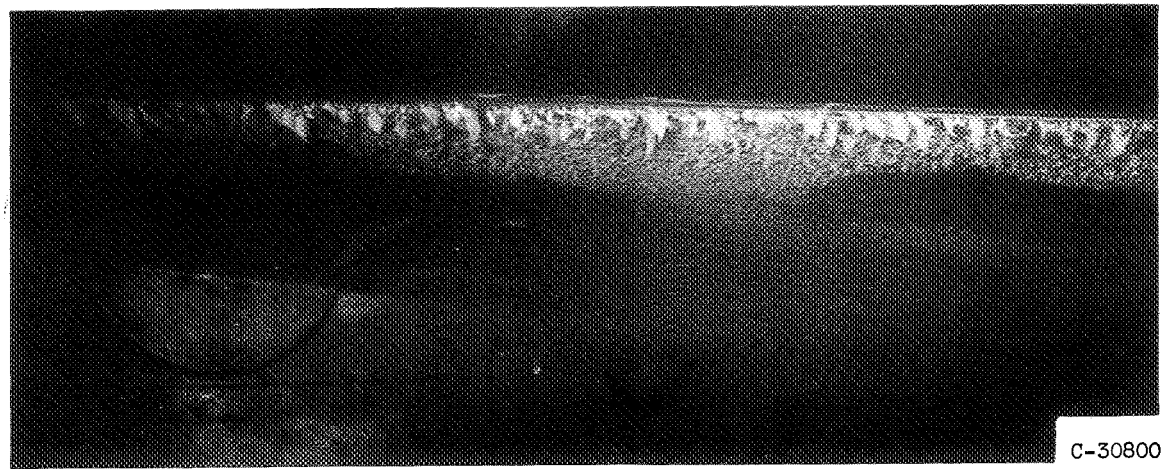

(b) Angle of attack, 6°; icing time, 5 minutes.

Figure 10. - Typical glaze-ice formation on airfoil. Airspeed, 275 miles per hour; datum air temperature, 25° F; liquid-water content, 0.85 gram per cubic meter.

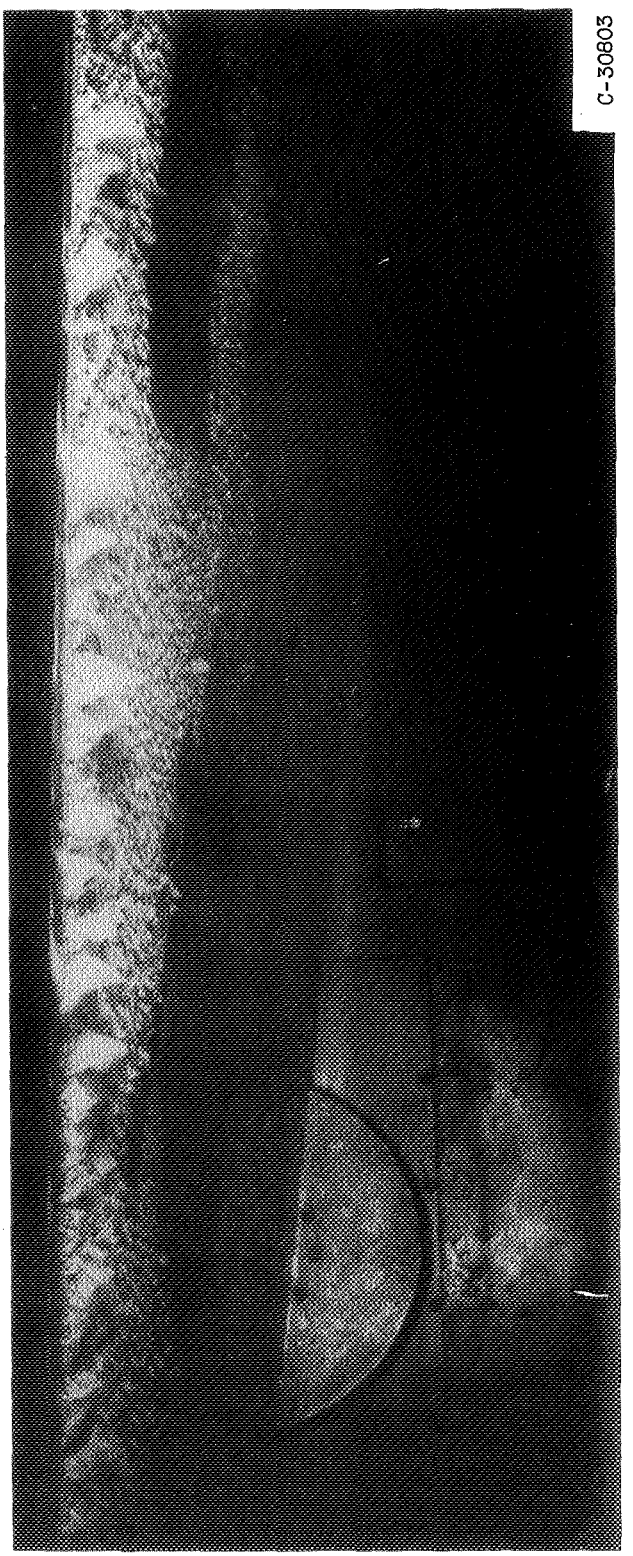

(c) Angle of attack, 6°; icing time, 11 $\frac{1}{2}$ minutes.

Figure 10. - Concluded. Typical glaze-ice formation on airfoil. Airspeed, 275 miles per hour; datum air temperature, 25° F; liquid-water content, 0.85 gram per cubic meter.

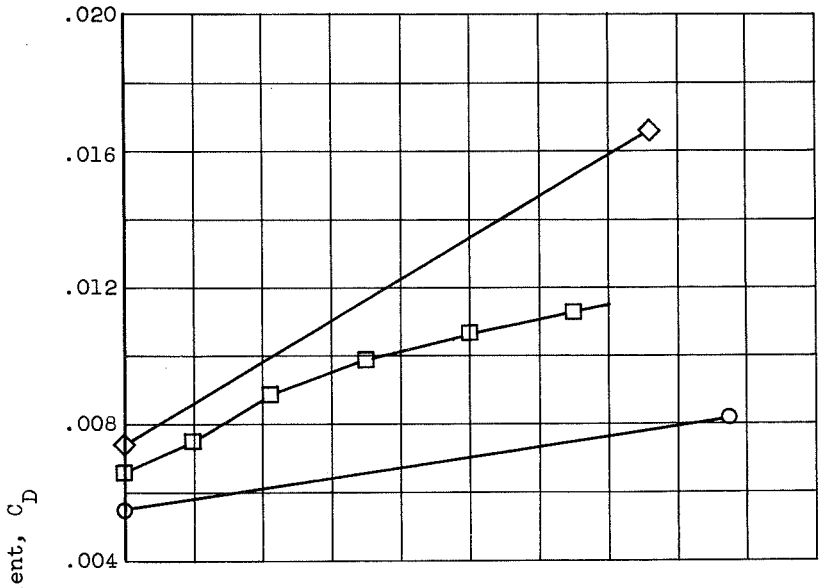

(a) Angle of attack, 2°.

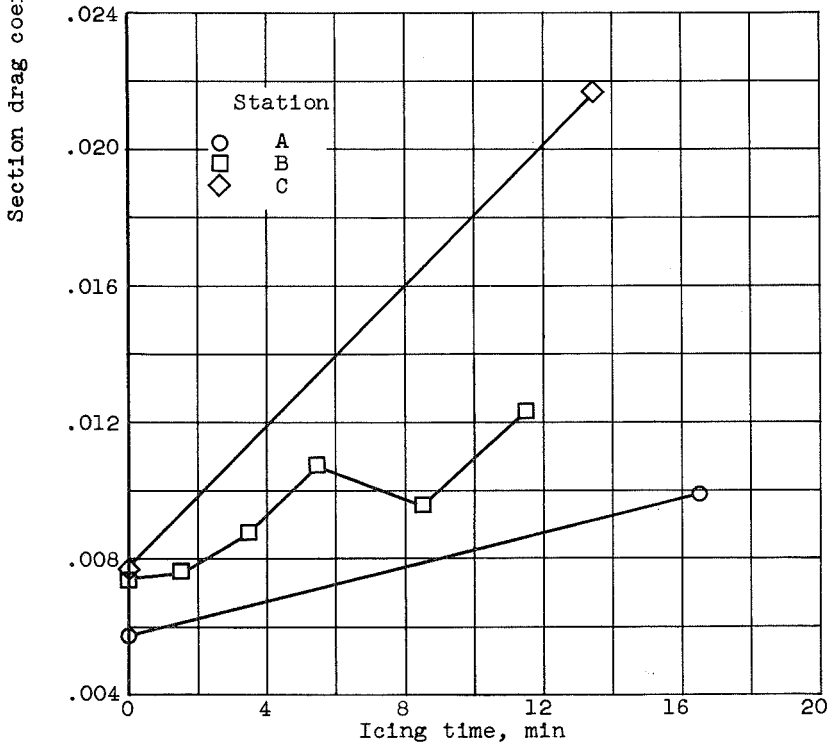

(b) Angle of attack, 4°.

Figure 11. - Variation of section drag coefficient with icing time for unheated leading-edge section with afterbody heated to prevent frost. Airspeed, 275 miles per hour; datum air temperature, 25° F; liquid-water content, 0.5 gram per cubic meter.

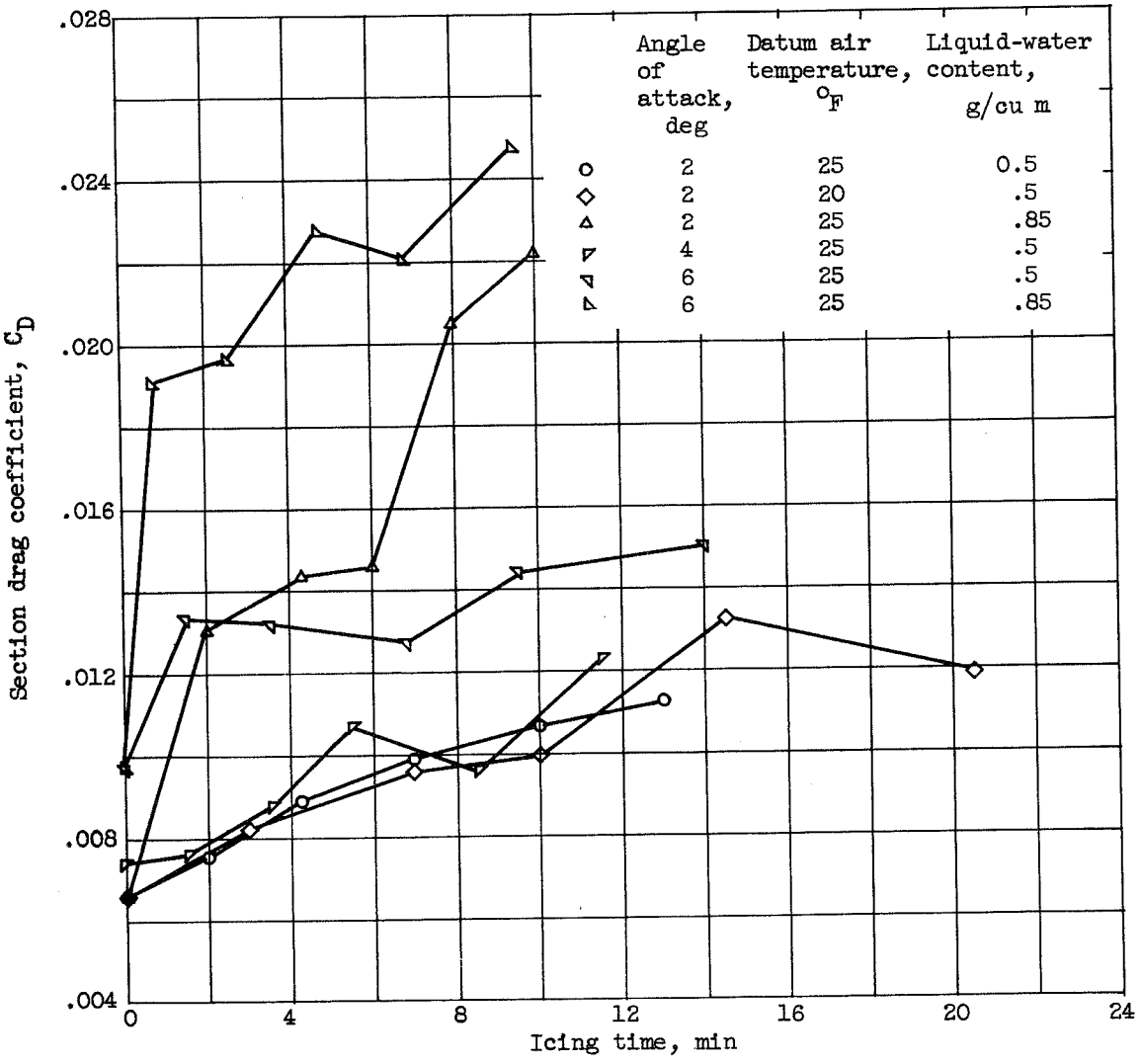

Figure 12. - Summary of icing drag data for station B with leading-edge section unheated. Airspeed, 275 miles per hour.

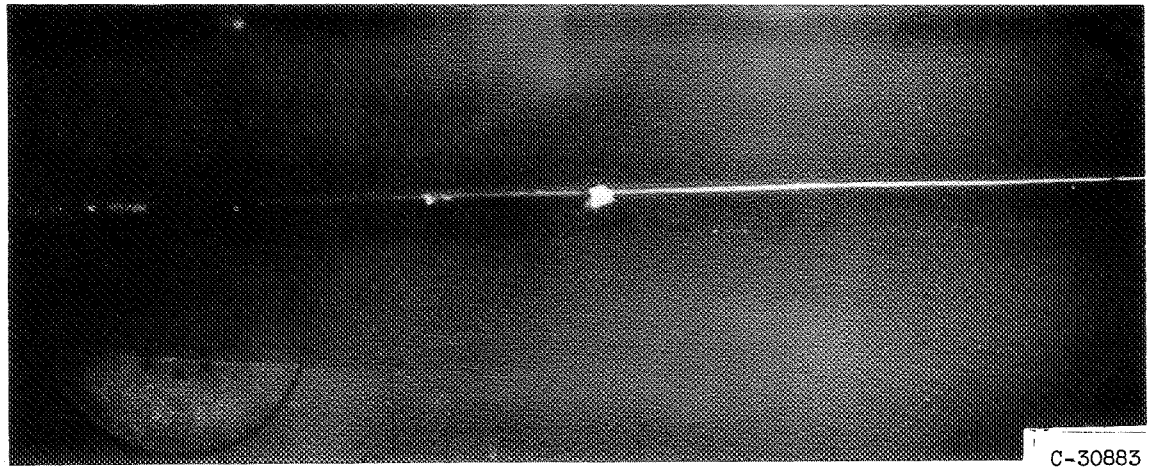

(a) Icing time, 9 minutes.

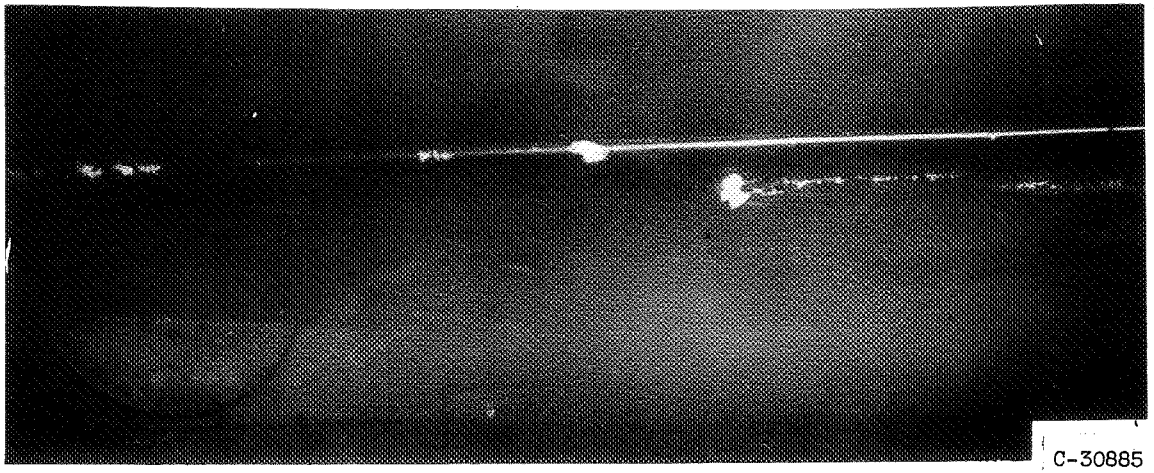

(b) Icing time, $26\frac{1}{2}$ minutes.

Figure 13. - Growth of residual ice formation on airfoil with submarginal heating. Airspeed, 275 miles per hour; datum air temperature, 25° F; angle of attack, 2°; liquid-water content, 0.7 gram per cubic meter.

CONFIDENTIAL

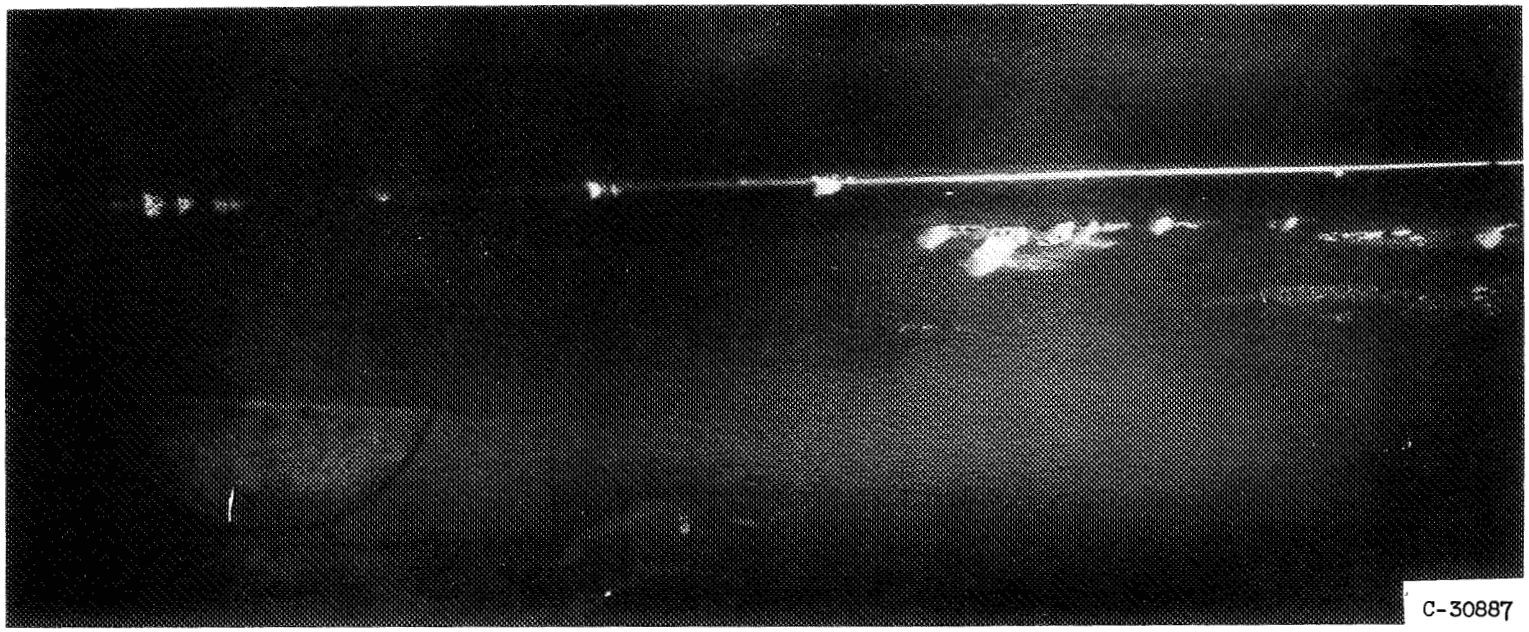

(c) Icing time, 34 minutes.

Figure 13. - Concluded. Growth of residual ice formation on airfoil with submarginal heating. Airspeed; 275 miles per hour; datum air temperature, 25° F; angle of attack, 2°; liquid-water content, 0.7 gram per cubic meter.

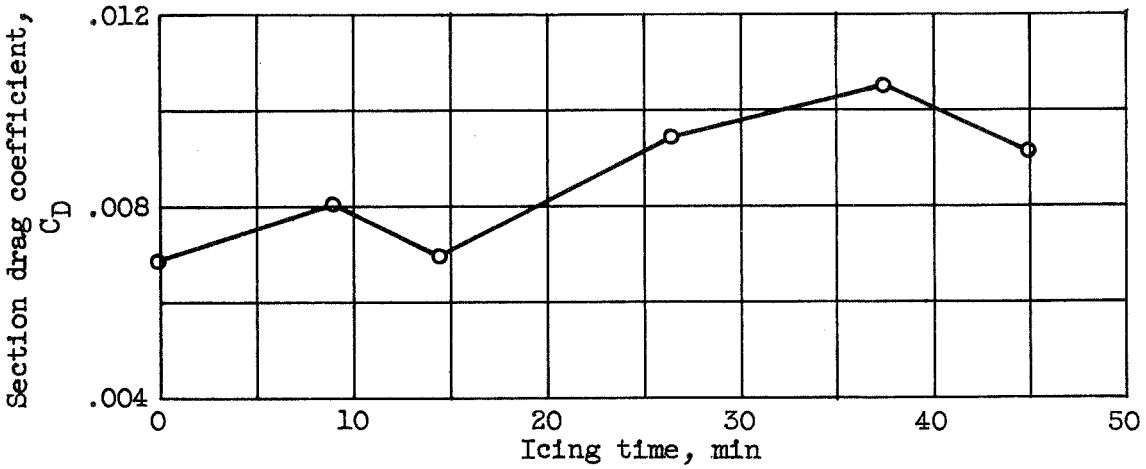

Figure 14. - Drag increase at station B with submarginal heating rate. Airspeed, 275 miles per hour; datum air temperature, 25° F; angle of attack, 2°; liquid-water content, 0.7 gram per cubic meter.

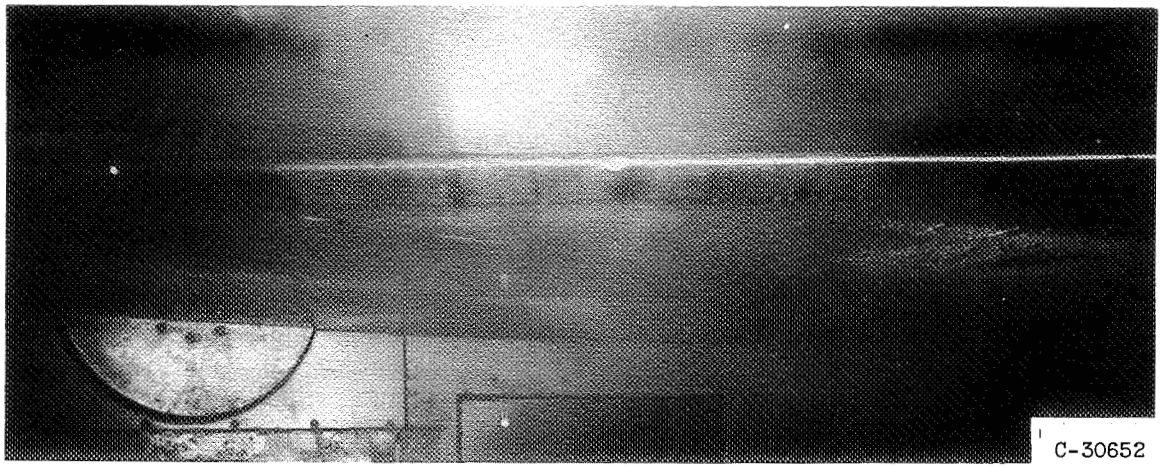

(a) Heating rate, 20,300 Btu per hour per foot span.

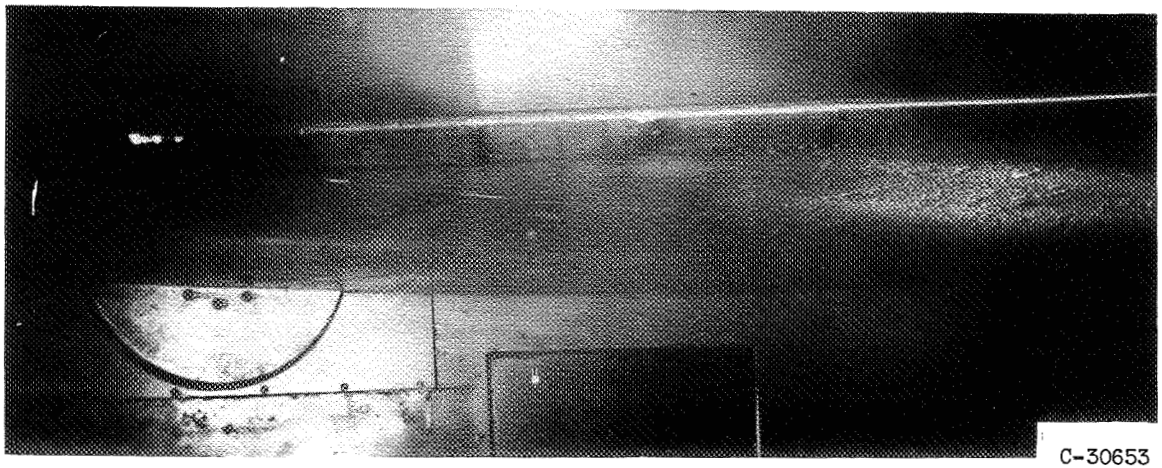

(b) Heating rate, 17,000 Btu per hour per foot span.

Figure 15. - Residual ice formations for various heating rates. Airspeed, 275 miles per hour; angle of attack, 2°; datum air temperature, 0° F; liquid-water content, 0.4 gram per cubic meter.

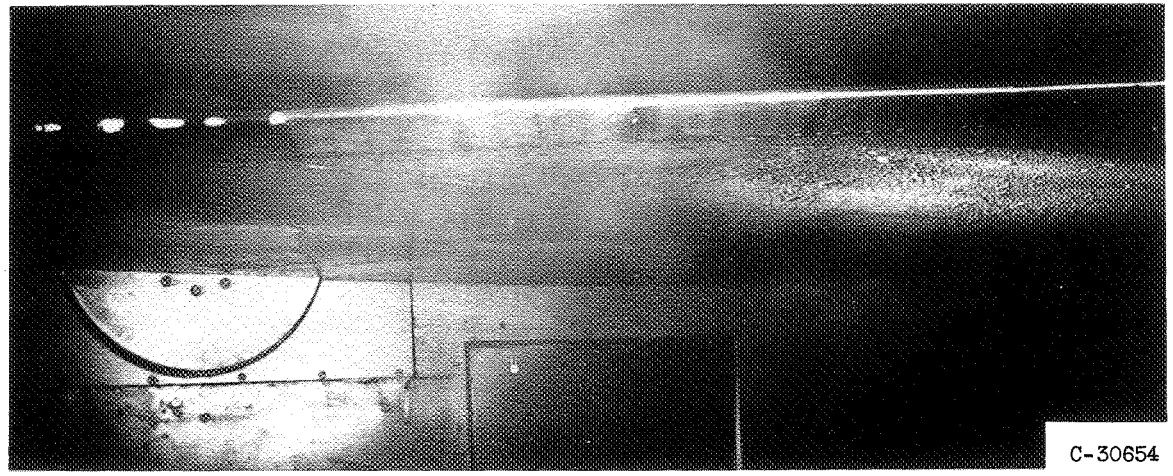

(c) Heating rate, 14,400 Btu per hour per foot span.

(d) Heating rate, 12,100 Btu per hour per foot span.

Figure 15. - Concluded. Residual ice formations for various heating rates. Airspeed, 275 miles per hour; angle of attack, 2°; datum air temperature, 0° F; liquid-water content, 0.4 gram per cubic meter.

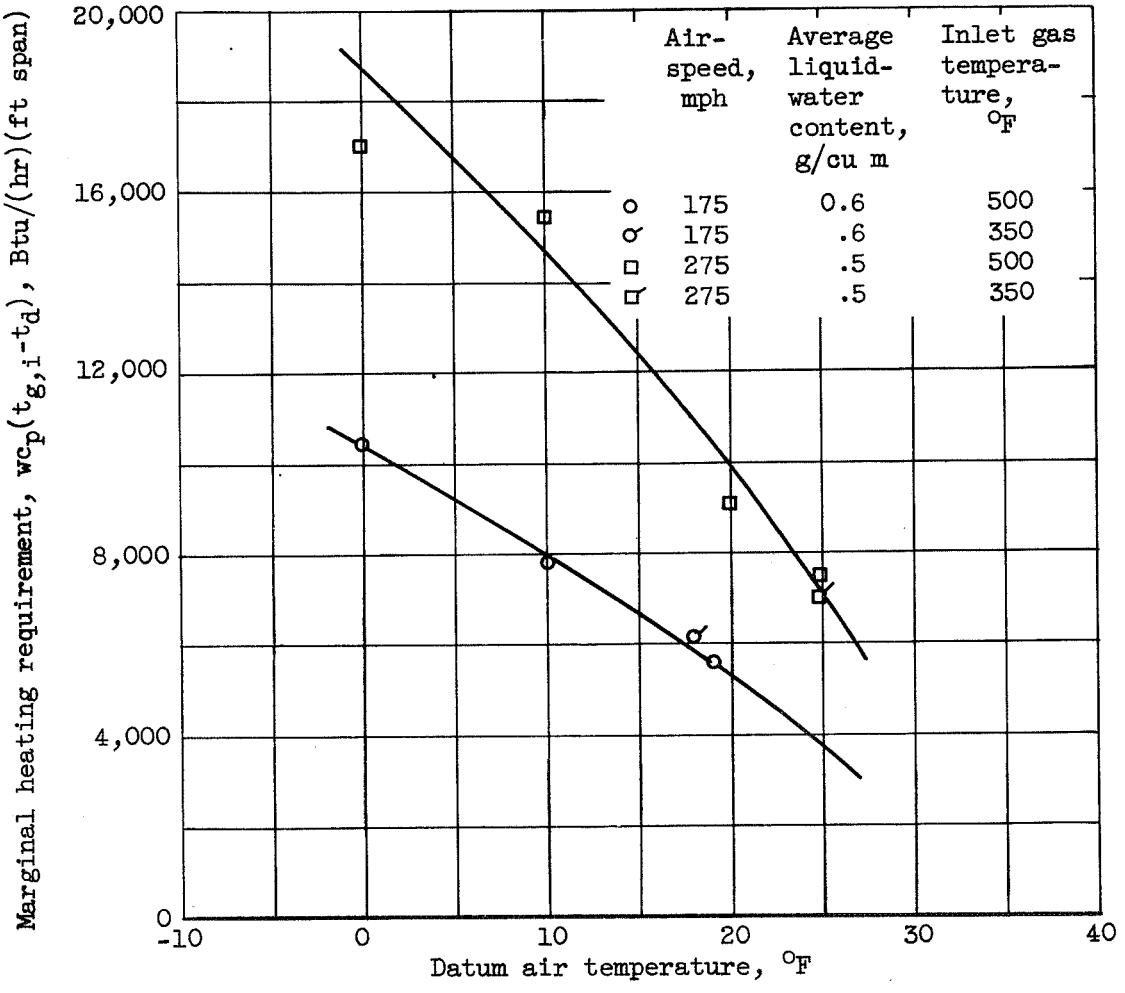

(a) Variation with datum air temperature. Angle of attack, 2°.

Figure 16. - Variation of marginal heating requirement with datum air temperature, angle of attack, and liquid-water content.

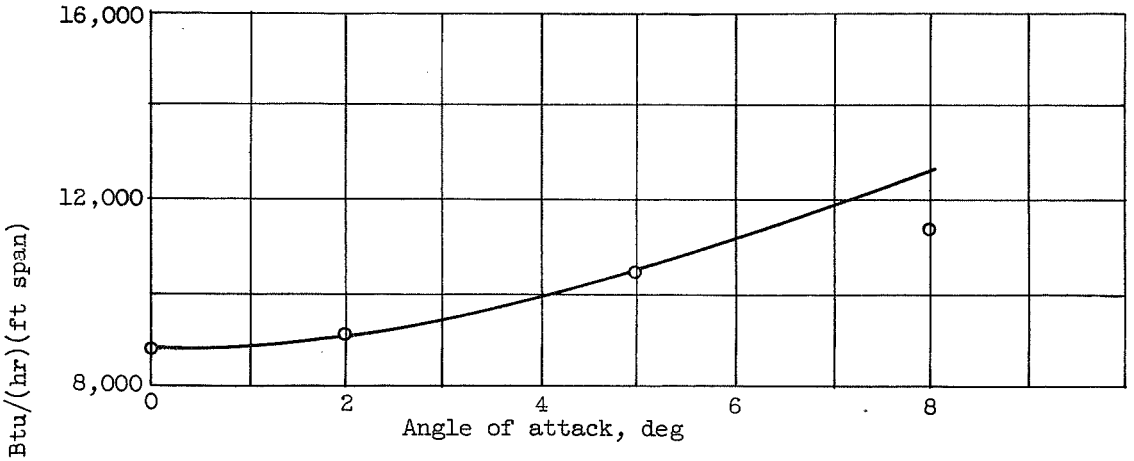

(b) Variation with angle of attack. Airspeed, 275 miles per hour; datum air temperature, 20° F; inlet gas temperature, 500° F; liquid-water content, 0.5 gram per cubic meter.

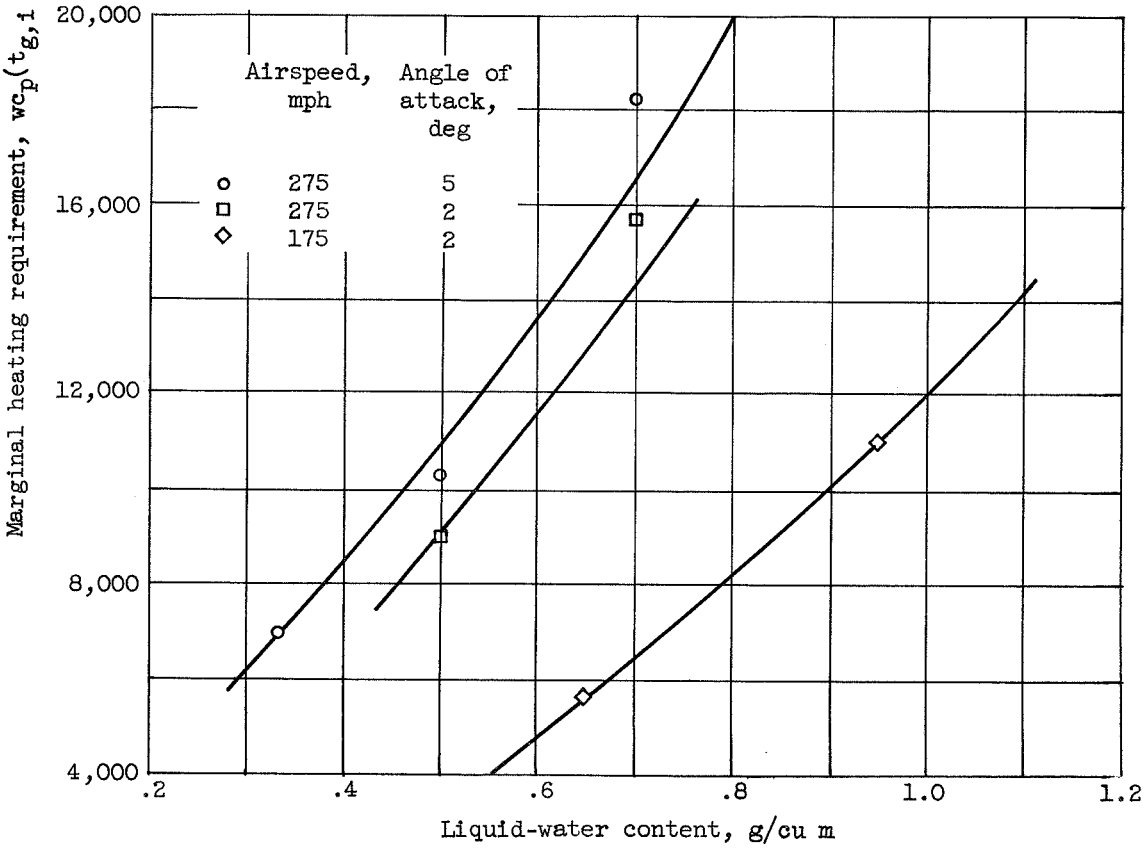

(c) Variation with liquid-water content. Datum air temperature, 20° F; inlet gas temperature, 500° F.

Figure 16. - Concluded. Variation of marginal heating requirement with datum air temperature, angle of attack, and liquid-water content.

(a) Airspeed, 275 miles per hour; angle of attack, 2°; datum air temperature, 25° F; liquid-water content, 0.5 gram per cubic meter; gas-flow rate, 70.3 pounds per hour per foot span; inlet gas temperature, 472° F.

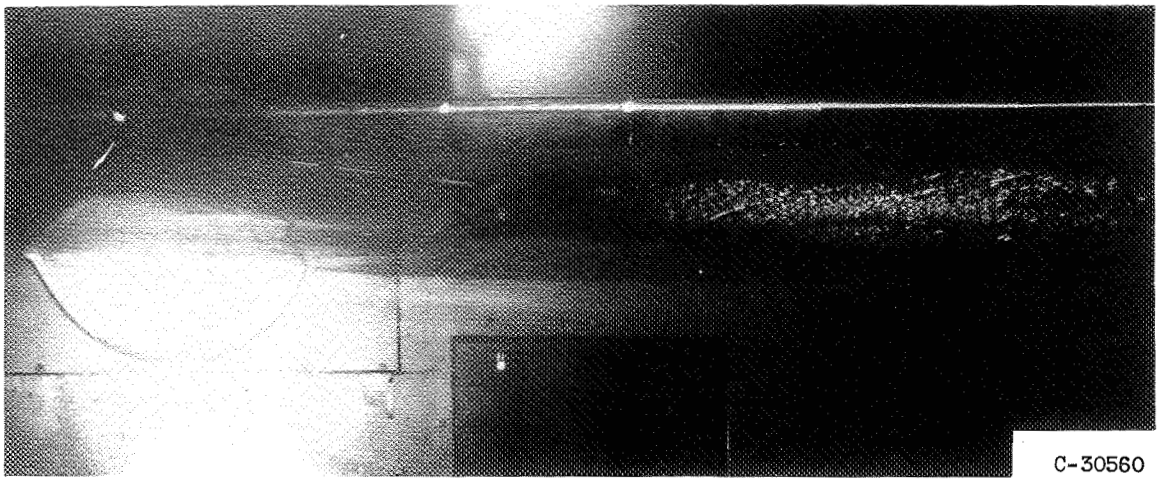

(b) Airspeed, 175 miles per hour; angle of attack, 2°; datum air temperature, 18° F; liquid-water content, 0.6 gram per cubic meter; gas-flow rate, 75.8 pounds per hour per foot span; inlet gas temperature, 354° F.

Figure 17. - Residual ice formations at marginal heating rate.

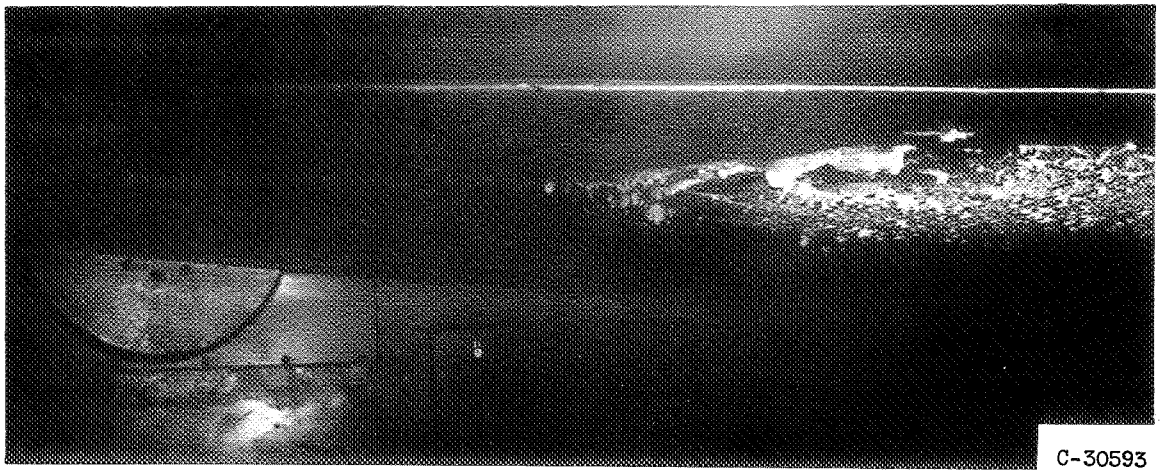

(c) Airspeed, 275 miles per hour; angle of attack, 5°; datum air temperature, 22° F; liquid-water content, 0.7 gram per cubic meter; gas-flow rate, 153 pounds per hour per foot span; inlet gas temperature, 519° F.

(d) Airspeed, 275 miles per hour; angle of attack, 8°; datum air temperature, 20° F; liquid-water content, 0.5 gram per cubic meter; gas-flow rate, 101.8 pounds per hour per foot span; inlet gas temperature, 488° F.

Figure 17. - Concluded. Residual ice formations at marginal heating rate.

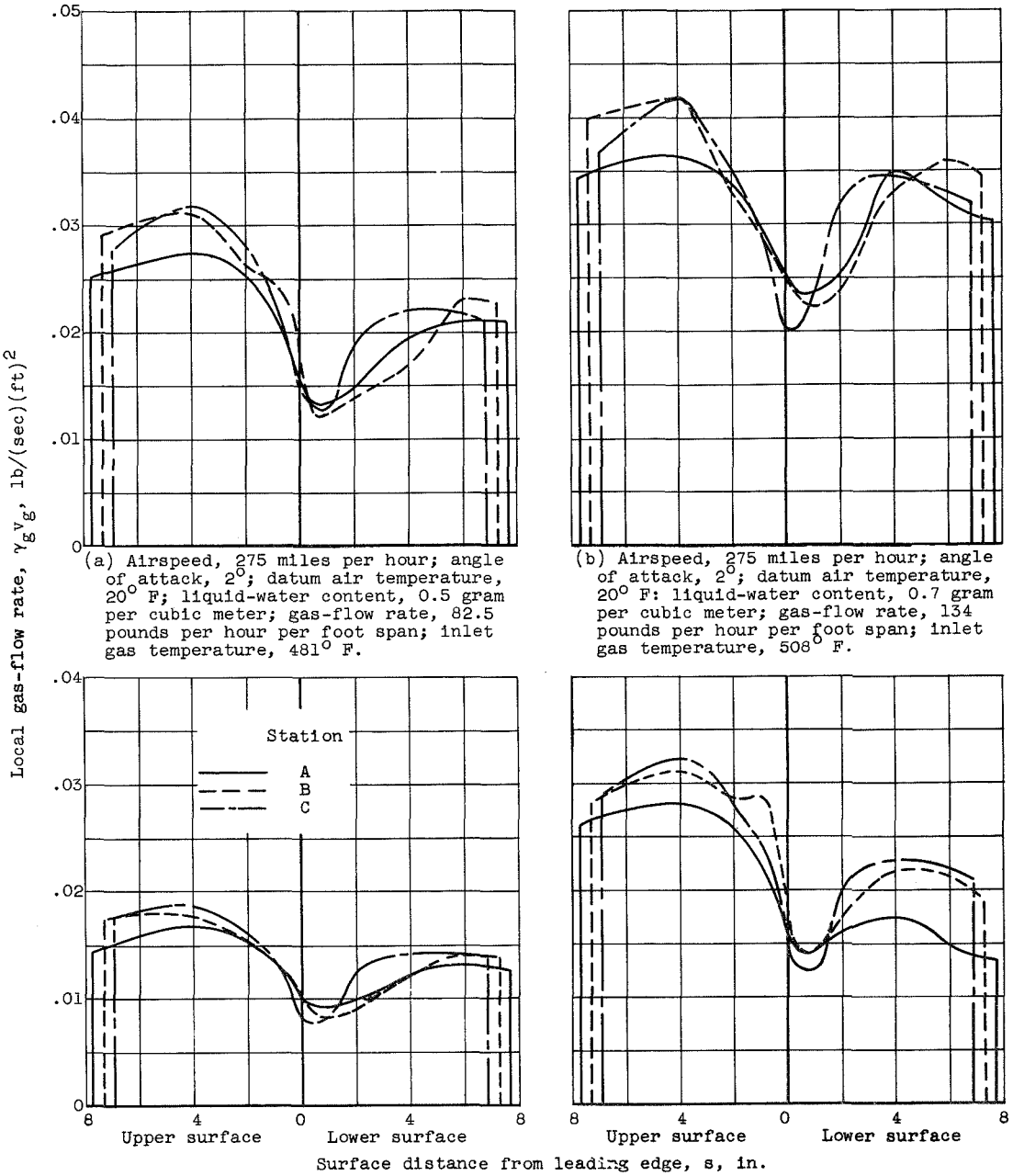

(a) Airspeed, 275 miles per hour; angle of attack, 2°; datum air temperature, 20° F; liquid-water content, 0.5 gram per cubic meter; gas-flow rate, 82.5 pounds per hour per foot span; inlet gas temperature, 481° F.

(b) Airspeed, 275 miles per hour; angle of attack, 2°; datum air temperature, 20° F: liquid-water content, 0.7 gram per cubic meter; gas-flow rate, 134 pounds per hour per foot span; inlet gas temperature, 508° F.

(c) Airspeed, 175 miles per hour; angle of attack, 2°; datum air temperature, 19° F; liquid-water content, 0.7 gram per cubic meter; gas-flow rate, 53 pounds per hour per foot span; inlet gas temperature, 458° F.

(d) Airspeed, 275 miles per hour; angle of attack, 2°; datum air temperature, 25° F; liquid-water content, 0.5 gram per cubic meter, gas-flow rate, 89.5 pounds per hour per foot span; inlet gas temperature, 350° F.

Figure 18. - Chordwise and spanwise variation of local gas-flow rate for marginal heating rate.

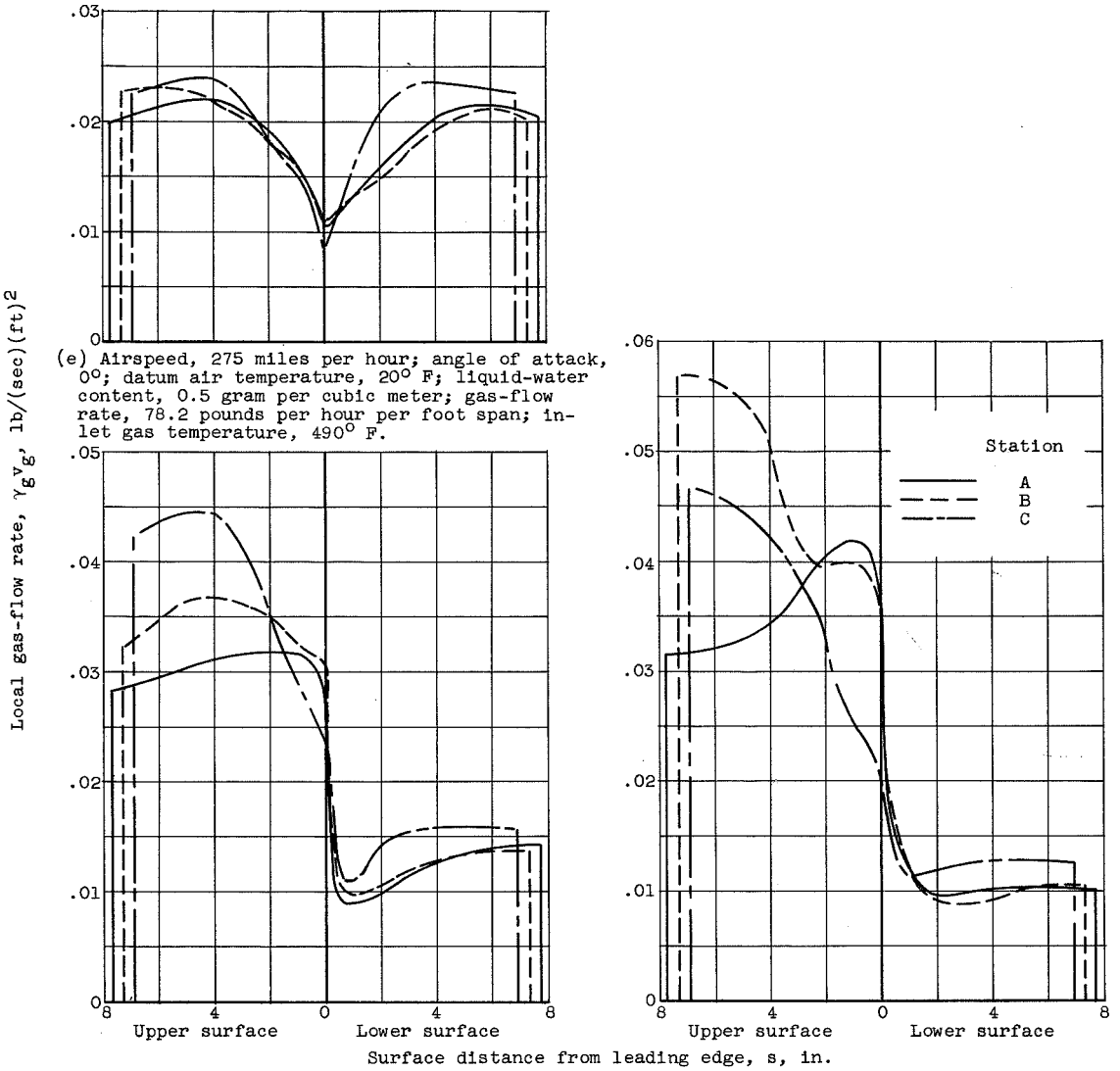

(e) Airspeed, 275 miles per hour; angle of attack, 0°; datum air temperature, 20° F; liquid-water content, 0.5 gram per cubic meter; gas-flow rate, 78.2 pounds per hour per foot span; inlet gas temperature, 490° F.

(f) Airspeed, 275 miles per hour; angle of attack, 5°; datum air temperature, 25° F; liquid-water content, 0.5 gram per cubic meter; gas-flow rate, 93.2 pounds per hour per foot span; inlet gas temperature, 486° F.

(g) Airspeed, 275 miles per hour; angle of attack, 8°; datum air temperature, 20° F; liquid-water content, 0.5 gram per cubic meter; gas-flow rate, 101.8 pounds per hour per foot span; inlet gas temperature, 488° F.

Figure 18. - Concluded. Chordwise and spanwise variation of local gas-flow rate for marginal heating rate.

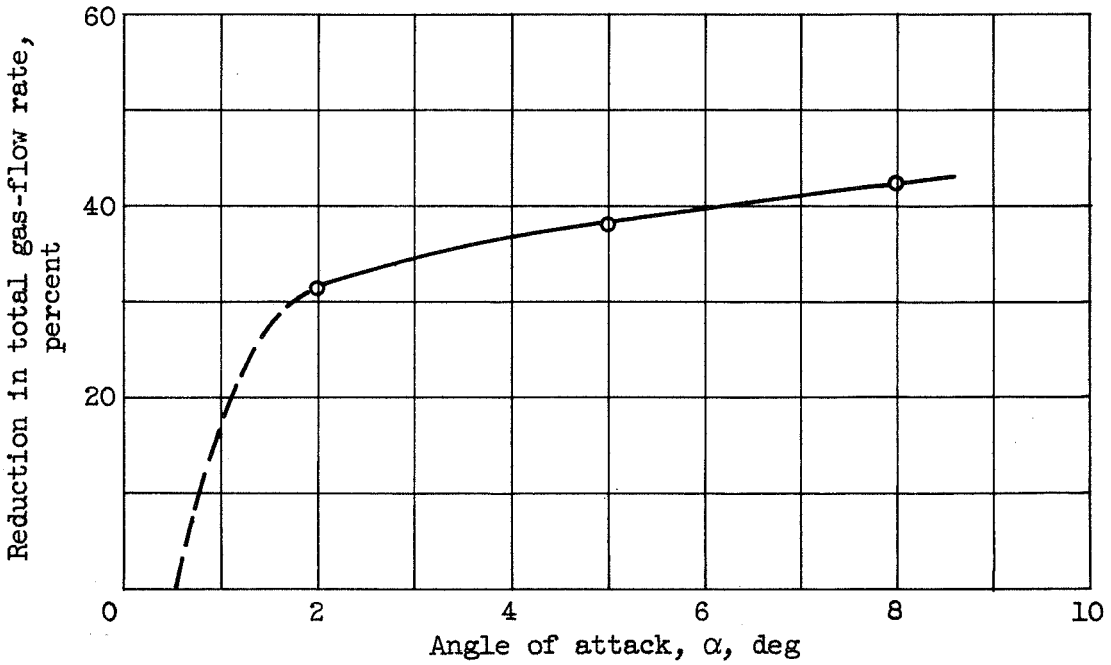

Figure 19. - Reduction in total gas-flow rate required for marginal anti-icing when distance heated on upper surface is reduced to one-half the distance on lower surface.

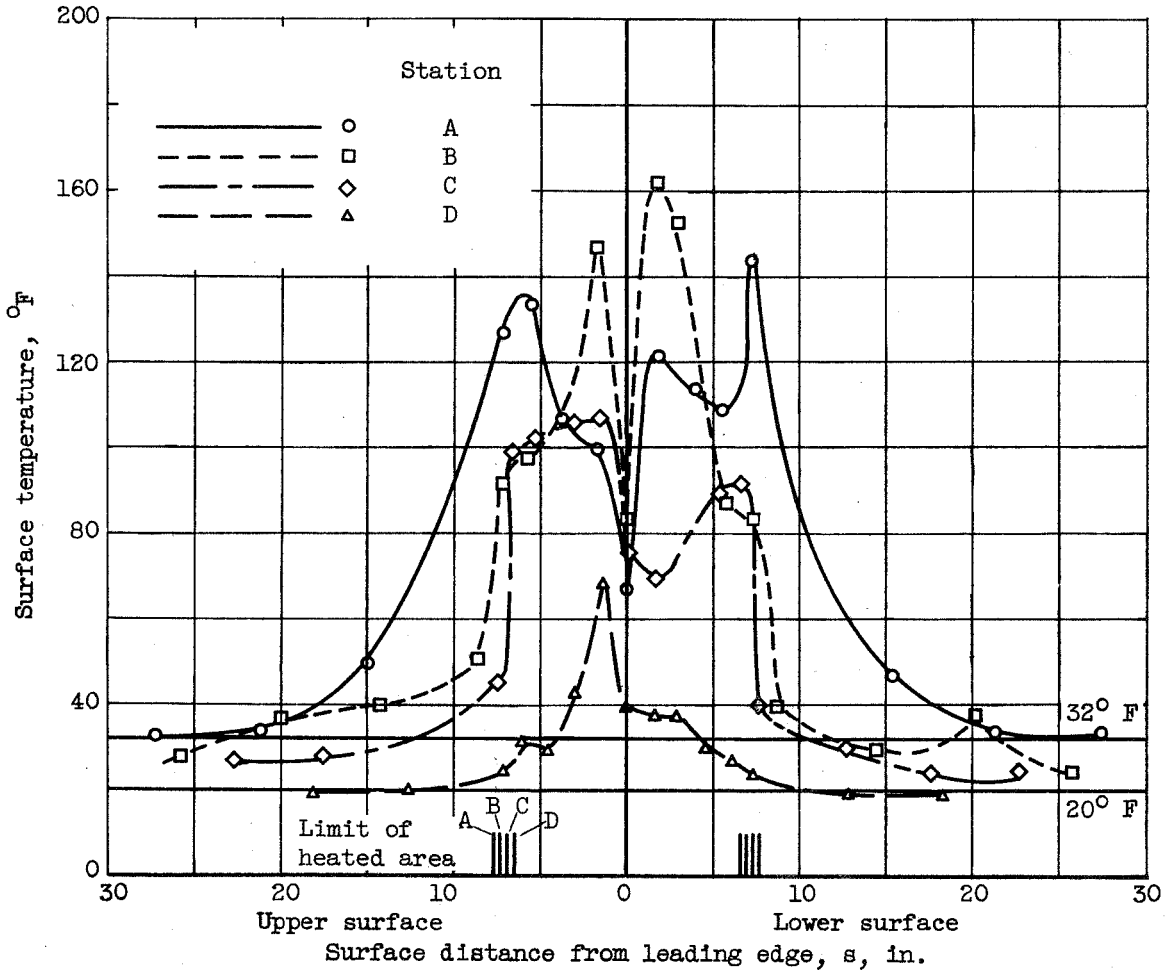

Figure 20. - Chordwise and spanwise surface-temperature variation in icing with marginal heating rate. Airspeed, 275 miles per hour; angle of attack, 2°; datum air temperature, 20° F; liquid-water content, 0.5 gram per cubic meter; gas-flow rate, 82.5 pounds per hour per foot span; inlet gas temperature, 481° F.

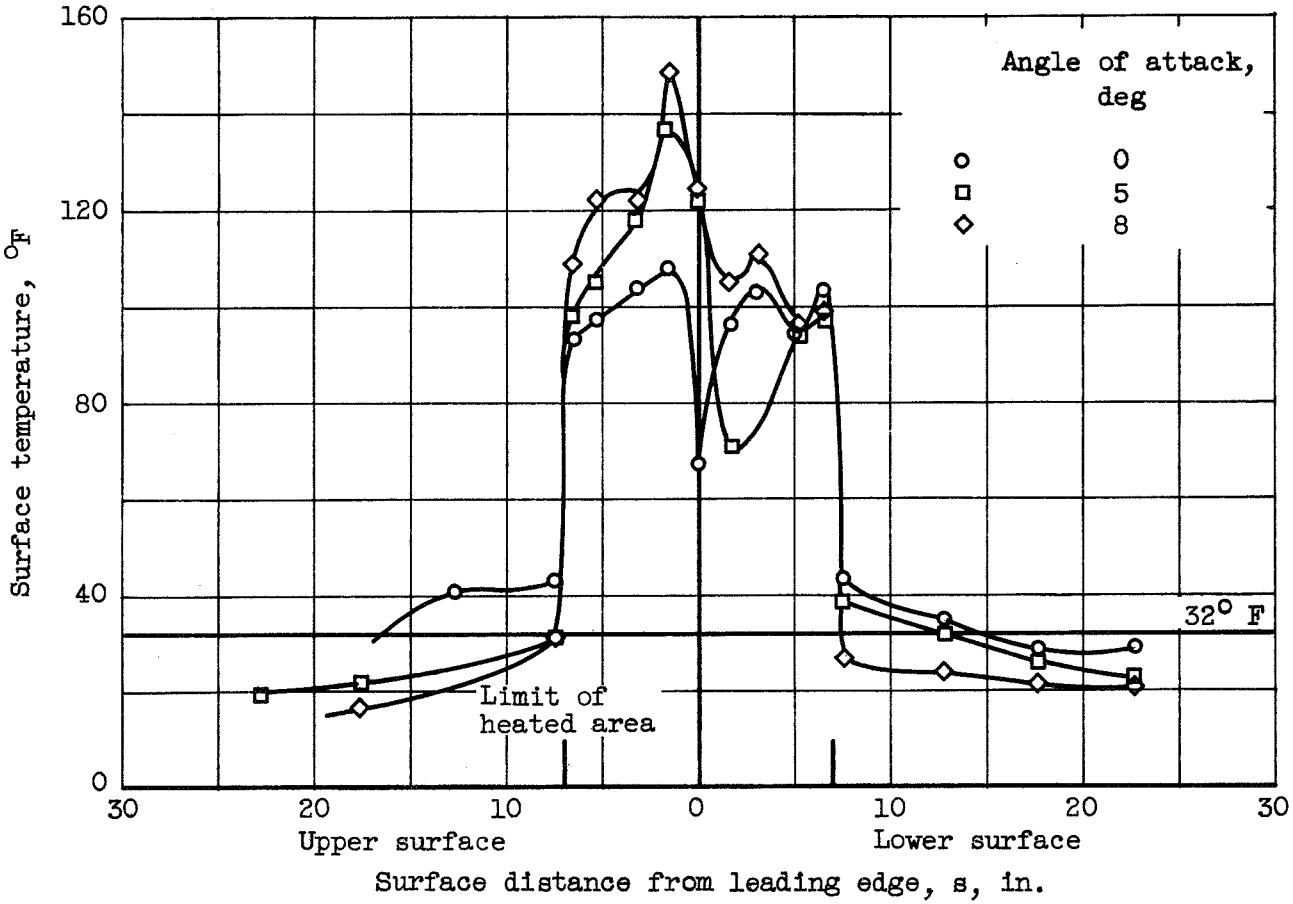

(a) Variation with angle of attack. Airspeed, 275 miles per hour; datum air temperature, 20° F; liquid-water content, 0.5 gram per cubic meter.

Figure 21. - Chordwise surface-temperature profiles at station C with marginal heating rate.

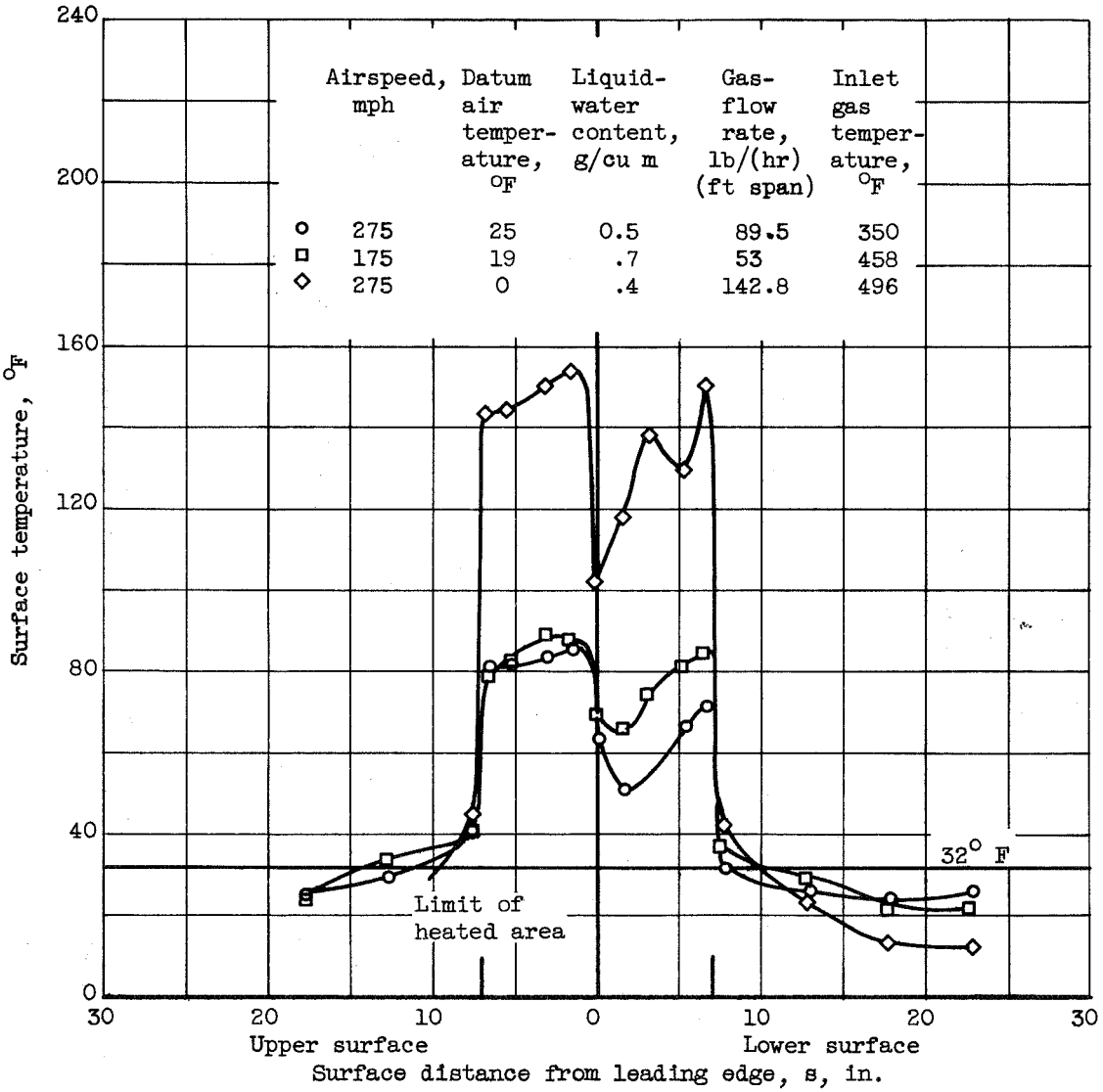

(b) Variation for three icing conditions at angle of attack of 2°.

Figure 21. - Concluded. Chordwise surface-temperature profiles at station C with marginal heating rate.

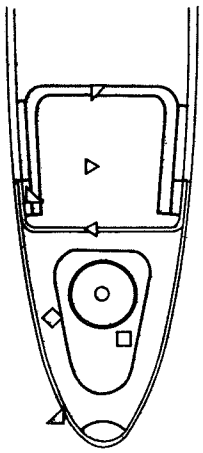

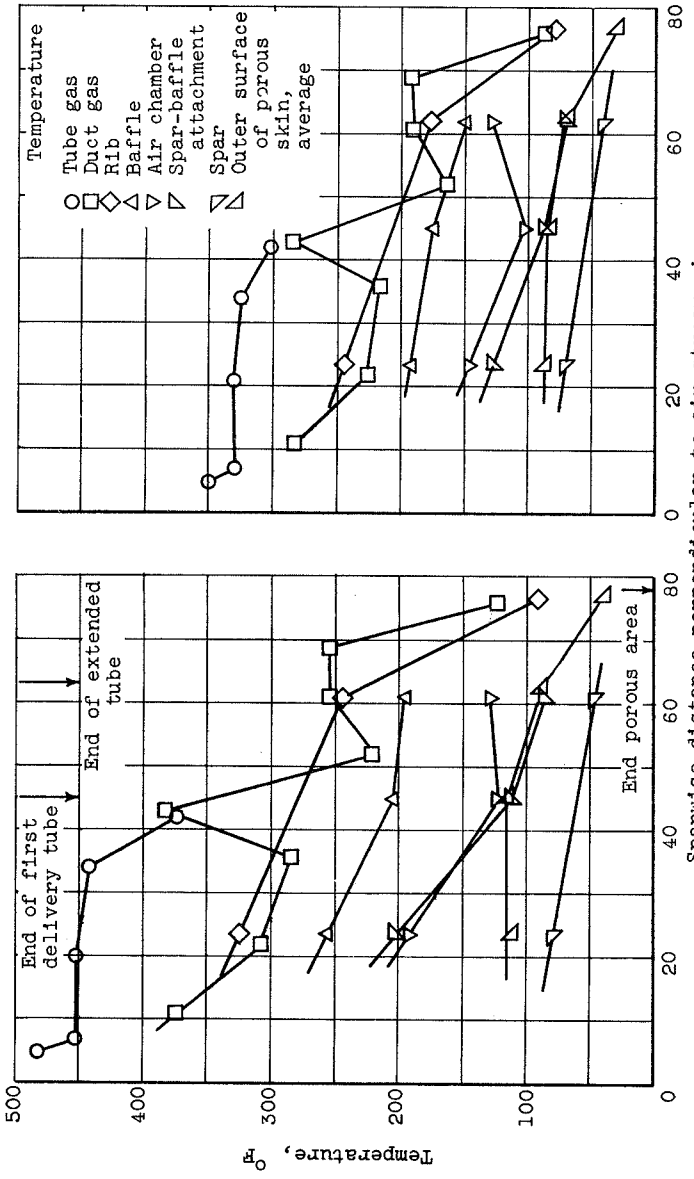

(a) Datum air temperature, 20° F; gas-flow rate, 82.5 pounds per hour per foot span; inlet gas temperature, 481° F.

(b) Datum air temperature, 25° F; gas-flow rate, 89.5 pounds per hour per foot span; inlet gas temperature, 350° F.

Figure 22. - Spanwise variation of internal gas and structural temperatures. Airspeed, 275 miles per hour; angle of attack, 2°; liquid-water content, 0.5 gram per cubic meter.

NACA-Langley - 1-19-55 - 325